Science & Global Security, 2000, Volume 8, pp.219–271
Reprints available directly from the publisher
Photocopying permitted by license only

Using Commercial Imaging Satellites to Detect the Operation of Plutonium-Production Reactors and Gaseous-Diffusion Plants

Hui Zhang and Frank N. von Hippel[a]

The operation of dedicated plutonium-production reactors and large gaseous-diffusion uranium-enrichment plants (GDPs), can be detected remotely using commercial observation-satellite imagery. Declassified Corona imagery is used to demonstrate that the new generation of commercial observation satellites with 1-meter spatial resolution will be able to detect vapor plumes inside and downwind from large operating natural-draft cooling towers. Low-resolution Landsat-5 thermal infrared images have been shown by other authors to be able to detect warm water discharges from reactors into lakes, rivers, etc. Here, the same systems are shown to be able detect the elevated temperature of the roofs of large operating GDPs. Commercial-satellite observations could therefore play an important role in increasing confidence in declarations that plutonium-production reactors and GDPs have been shut down as a result of a fissile-material-production moratorium or Fissile Material Cutoff Treaty.

a Hui Zhang is a research fellow at the Belfer Center for Science and International Affairs, at Harvard University's Kennedy School of Goverment. Frank N. von Hippel is a Professor of Public and International Affairs at Princeton University. More details may be found in Hui Zhang and Frank von Hippel, "The Application of Commercial Observation Satellite Imagery for the Verification of Declared and Undeclared Plutonium Production Reactors"; and "Using Commercial Observation Satellites to Verify that Gaseous-diffusion Uranium-enrichment Plants are not Operating" [Princeton University, Center for Energy and Environmental Studies Reports: PU/CEES 319 (1999) and PU/CEES 325 (2000). http://www.princeton.edu/~cees/arms/].

INTRODUCTION

A Fissile Material Cutoff Treaty (FMCT) that would allow on-site verification of a ban on the production of plutonium and highly-enriched uranium (HEU) for weapons will probably not come into force for some years. However, four of the nuclear-weapon states (the U.S., Russia, Britain and France) have announced that they have ended their production of plutonium and HEU for weapons and China has privately communicated that it has not been producing these materials for weapons since approximately 1991. The other nations (Israel, India and Pakistan), which have not joined the NPT as non-weapon states, are being pressed to join in this production moratorium.[1]

Strengthening confidence in such declared production moratoria would be desirable. In many cases, this could be done by remote confirmation that former production facilities are not operating. This paper explores the extent to which the shutdown of plutonium-production reactors and uranium enrichment plants could be confirmed using commercial observation satellite imagery.

Plutonium-production reactors

Although any reactor can be used to produce plutonium, virtually all plutonium for weapons appears to have been produced in dedicated production reactors (see table 1). In some cases these reactors have been dual-purpose, producing electric power as well as plutonium. In some cases they have been used to produce other isotopes for military and civilian purposes. But, in most cases, plutonium-production reactors have been shut down when countries have halted plutonium production.

Specifically, most U.S., Russian, and French plutonium-production reactors have been shut down. Three Russian plutonium-production reactors still operate to provide heat to regional populations. The U.S. and Russia have a still-to-be-fully implemented agreement under which these reactors are to be shut down or converted to a fuel that does not have to be reprocessed. As part of this agreement, the two countries have also agreed to reciprocally monitor the status of their shutdown reactors and to confirm that new plutonium produced by three still-operating Russian plutonium-production reactors is not diverted to weapons use. Britain still operates eight small plutonium-production reactors to generate electrical power and tritium and France still operates the Phénix demonstration breeder reactor that may in the past have produced plutonium for weapons. However, all plutonium-separation activities in Britain and France are now subject to Euratom safeguards.

China has not announced specifically that it has shut down its plutonium-production reactors but reportedly shut down at least one in 1984 before it

suspended plutonium-production for weapons entirely in 1991.[2]

Table 1: Plutonium-production reactors of the world and their cooling systems

UNITED STATES				
Reactors	Reactor Type[a]	Status	Peak Power (GWt)	Cooling System
Hanford Reservation				
8 Reactors: B,D,F,DR,H & C KW & KE	LWGR	Permanently shutdown:[b] and partially dismantled	2.5 4.4	Once through; hot water discharged into Columbia River
N-Reactor	LWGR	Dual use (electric power), startup 12/31/63; in cold standby since 1987, deactivation initiated.	4	"
Savannah River Site				
K reactor	HWR	Startup: 10/51: in cold standby since 1988 with no plans for operation,	2.71	Natural draft hyperbolic cooling tower
Reactors: P R	HWR	Permanently shutdown[c]	2.68 2.26	Both reactors discharged their hot water into a cooling pond
Reactors: C L	HWR	Permanently shutdown[c]	2.915 2.7	Once-through cooling: hot water discharged into Savannah River through streams and swamps

[a] LWGR: Light-water-cooled, graphite-moderated reactor; HWR: Heavy-Water Reactor; GCR: gas-cooled, graphite-moderated reactor; FBR: fast-neutron, sodium-cooled breeder reactor.
[b] Operating dates: B (9/44-2/12/68), D (12/44-6/26/67), F (2/45-6/25/65), DR (10/50-12/30/64), H (10/49-4/65), C (11/52-4/25/69); KW (1/55-2/1/70), KE (4/55-1/28/71).
[c] Operating dates: P (2/54-1989) R (12/53-6/15/64); C (3/55-1989), L-reactor (7/54-2/18/68)

Table 1 (Continued)

RUSSIA				
Sites	Reactor Type	Status	Peak Power (GWt)	Cooling System
Ozersk (Chelyabinsk-65)				
5 Reactors: A IR AV-1, AV-2 & AV-3	LWGR	Permanently shutdown[d]	0.5 0.065 2.09	All with once-through cooling, discharge into Lake Kyzyltash
Seversk (Tomsk-7)				
3 Reactors: I-1,EI-2 ADE-3	LWGR	Permanently shutdown[e]	1.2 1.9	I-1 reactor: once-through cooling, discharge into the Romashka Creek and then Tom River; EI-2 and ADE-3, natural draft hyperbolic cooling towers
2 reactors: ADE-4, ADE-5	LWGR	Operating since 65 and 68: producing heat and electricity for Seversk and Tomsk	1.9	Natural draft hyperbolic cooling towers
Zhelenznogorsk (Krasnoyarsk-26)				
Reactors: AD, ADE-1	LWGR	Permanently shutdown[f]	2	Once through cooling with Yenisey River cooling water
Reactor: AD-2	LWGR	Operating since 64; producing heat and electricity for Zhelenznogorsk	2	The secondary cooling loop uses once-through Yenisey River cooling water

[d] Operating dates: A (6/22/48-87), IR (12/22/51-5/24/87), AV-1 (7/15/50-8/12/89), AV-2 (4/6/51-7/90), AV-3 (9/15/52-11/1/90)

[e] Operating dates: I-1 (11/20/55-8/21/90), I-2 (9/58-12/28/90), ADE-3 (7/14/61-8/14/92)

[f] Operating dates: AD (9/25/58-6/30/92), ADE-1 (7/20/61-9/29/92)

Table 1 (Continued)

UNITED KINGDOM				
Site	Reactor Type	Status	Peak Power (GWt)	Cooling System
Sellafield 2 Windscale Piles		Being decommissioned[g], operated 1951-57	--	
4 Calderhall reactors	GCR	Operable, dual use (electric power)[h]	0.24	Natural draft hyperbolic cooling towers
Chapelcross 4 Chapelcross reactors	GCR	Operable, dual use (electric power)[h]	0.24	Natural draft hyperbolic cooling towers

[g] http://www.ukaea.org.uk/oindex.htm
[h] The Calder Hall reactors began full-power operation in 10/56, 2/57, 5/58, and 2/59; the Chapel Cross reactors in 2/59, 9/59, 11/59, and 3/60. See also http://www.bnfl.com/BFNL Website.nsf/HTML/CompanyProfile/OpenDocument

Table 1 (Continued)

FRANCE				
Site	Reactor Type	Status	Peak Power (GWt)	Cooling System
Marcoule complex reactors				
G1	GCR	G1 and G2 decommissioned; G3 permanently shutdown[i]	0.40	--
G2			0.25	
G3			0.25	
Celestin - 1,2 reactors	HWR	Alternating in operation; producing only tritium since 1991; operating since 67,68	0.19	--
Others				
Chinon				
A1	GCR	Permanently shutdown[j]	0.30	--
A2			0.80	
A3			1.56	
Bugey 1	GCR	Permanently shutdown, operated 1972-94	1.85	--
St. Laurent				
A1	GCR	Permanently shutdown, operated 69-90, 71-92	1.65	--
A2			1.77	
Phenix	FBR	Operating since 74	0.567	--

[i] Operating dates: G1 (56-68), G2 (59-80), G3 (59-84)
[j] Operating dates: Chinon 1 (62-73), Chinon 2 (65-85), Chinon 3 (67-90)

CHINA				
Site	Reactor Type	Status	Peak Power (GWt)	Cooling system
Jiuquan Complex				
Jiuquan Reactor	LWGR	shutdown; operated 66-84?	≤0.5	six natural draft hyperbolic cooling towers
Guangyuan Complex				
Guangyuan Reactor	?	shutdown; operated 73-91?	≤1	?

Table 1 (Continued)

ISRAEL				
Site	Reactor Type	Status	Peak Power (GWt)	Cooling System
Dimona Complex				
Dimona Reactor	HWR	In operation since 12/63	≤0.07?	Mechanical draft cooling tower

INDIA				
Site	Reactor Type	Status	Peak Power (GWt)	Cooling System
Bhabba Atomic Research Center				
Cirus Reactor	HWR	In operation since 60	0.04	Once through into bay
Dhruva Reactor	HWR	In operation since 8/8/85; also produces neutron beams and radioisotopes for research and medicine	0.1	"

Table 1 (Continued)

PAKISTAN				
Site	Reactor Type	Status	Peak Power (GWt)	Cooling System
Khushab Reactor	HWR	In operation since 1998?	0.04-0.07	Mechanical draft cooling tower

Sources: U.S. Nuclear Weapons Databooks: III, Thomas B. Cochran, William M. Arkin, Robert S. Norris, and Milton M. Hoenig, Nuclear Warhead Facility Profiles (Ballinger, 1987); and IV. Robert S. Norris, Andrew S. Burrows and Richard W. Fieldhouse, British, French and Chinese Nuclear Weapons (Westview, 1994); Thomas B. Cochran, Robert S. Norris and Oleg Bukharin, Making the Russian Bomb: From Stalin to Yeltsin (Westview, 1995); David Albright, Frans Berkhout and William Walker, Plutonium and Highly Enriched Uranium 1996 (Oxford, 1997); NUKEM Market Report: World Nuclear Capacity, December 1993; also see http://www.insc.anl.gov/nre/nre.html; http://www.fas.org/nuke/guide/.

Uranium-enrichment plants

The world's stockpile of HEU has also been produced in a relatively small number of facilities (see Table 2). Some of these have been shut down and others are expected to shut down in the not-too-distant future. The plants being shut down are gaseous-diffusion enrichment plants (GDPs), because they are energy inefficient and therefore much more costly to operate than the uranium-centrifuge enrichments plants (CEPs) with which they are being replaced. Because Russia is providing the technology, China's replacement CEPs will be under international safeguards.

Table 2: Principal facilities used to produce HEU for weapons, worldwide

Site	Area (main building)	Status (dates of op.)	Capacity in 10^6kgSWU/y (stages)	Cooling System
UNITED STATES				
Oak Ridge		Shutdown in 1985	7.7	Cooling towers (wet,mechanical draft)
K-25	16.2ha.	HEU (1945-64)	(2996)	"
K-27	3.5ha.	HEU (1946-64)	(540)	"
K-29	2.7ha.	LEU (1951-85)	(300)	"
K-31	6.9ha.	LEU (1951-85)	(600)	"
K-33	13.1ha.	LEU (1954-85)	(640)	"
Paducah		In operation (Up to 2% LEU)	11.3	Cooling towers (wet,mechanical draft)
C-310	0.5ha.	(1953---)	(60)	"
C-331	4.7ha.	(1953---)	(400)	"
C-333	4.7ha.	(1954---)	(400)	"
C-335	10.0ha.	(1953---)	(480)	"
C-337	10.0ha.	(1954---)	(472)	"
Portsmouth		In operation (HEU prod. ended 1993)	8.3	Cooling towers (wet,mechanical draft)
X-326 (product)	11.0ha (2230X552ft)	(1956-93;93-partial)	(2340)	"
X-330	12.50ha. (2176X640ft)	(1955--)	(1100)	"
X-333 (feed)	12.7ha (1456X970ft)	(1955--)	(640)	"

Table 2 (Continued)

RUSSIA				
Site [a]	Area (main building)	Status (dates of op.)	Capacity in 10^6kgSWU/y	Cooling System
Sverdlovsk-44				
GDP	1100x70m	Established during 49-50s, 60s-90s, replaced by CEP		Once-through cooling, discharge to two huge artificial lakes.
CEP		In operation	9.8	--
Krasnoyarsk-45				
GDP	1000x50	Established during 1950s, 60s-90s replaced by CEP		Once-through cooling: discharge to River Kan
CEP	"	In operation	5.8	--
Angarsk				
GDP	1200x70m	Established during 1950s, 60s-90s replaced by CEP		Once-through cooling, discharge to Angara River
CEP	"	In operation	1.6	--
Tomsk-7				
GDP	750x70m	Established during 1950s, 60s-90s replaced by CEP		Once-through cooling, discharge to Tom's River
CEP	"	In operation	2.8	--

a: GDP: gasous diffusion plant;CEP: centrifuge enrichment plant

Table 2: (Continued)

UNITED KINGDOM				
Site	Area (main building)	Status (dates of op.)	Capacity in 10^6kg-SWU/y	Cooling System
Capenhurst GDP	?	Shutdown (cleaning and dismantling begun in 1982)	0.1-0.15	Cooling towers (natural draft)
CEP A3		Began operation in 1977. Since 1993, operated by Urenco under IAEA and Euratom safeguards, producing only LEU.	0.2	
EP-Urenco		Began in 1980. Under IAEA and Euratom safeguards from beginning. Making only LEU.	0.75	

Table 2 (Continued)

FRANCE				
Site	Area (main building)	Status (dates of op.)	Capacity in 10^6kgSWU/y	Cooling System
Pierrelatte				
GDP (plant has four buildings for: low, med, high and very-high enrichment)		Shutdown Began operations in 1967. Shutdown announced June 30, 1996.	0.4-0.6	?
Tricastin				
Georges Besses GDP, owned by Eurodif		In operation since 1979 producing less than 5% enriched LEU (belongs to Eurodif).	10.8	Cooling towers (wet, natural draft)

CHINA				
Site	Area (main building)	Status (dates of op.)	Capacity in 10^6kgSWU/y (stages)	Cooling System
Lanzhou				
GDP	600mx60m	Shutdown Began operation in 1963; HEU production ended in 1987	0.3	Cooling towers (wet, mechanical draft)
Heping				
GDP	?	Shutdown? Began operation in 1974; HEU production ended in 1987	0.15-0.59	?

Table 2 (Continued)

PAKISTAN				
Site	Area (main building)	Status (dates of op.)	Capacity in 10^6kgSWU/y (stages)	Cooling System
Kahuta				
CEP	--0.1ha.	Operating Began operation in mid-1980s	0.009-0.015	--

Note: 1ha.=10^4m^2.

Sources: David Albright, Frans Berkhout and William Walker, Plutonium and Highly Enriched Uranium 1996: World Inventories, Capabilities and Policies (Oxford University Press, 1997); Nuclear Weapons Databook, Volumes II and IV; Brookhaven National Laboratory, Transparancy Measures for DOE SNM Production Facilities, SSN 93-7, Dec. 1993; J. Merriman and M. Benedict, Recent Development in Uranium Enrichment, 221Vol.78, 1982, (American Institute of Chemical Engineers, New York); and Allan S. Krass, et. al., Uranium Enrichment and Nuclear Weapon Proliferation, (Taylor & Francis Inc., New York, 1983.)

The purpose of this paper is to explain how confidence in the shutdown of plutonium-production reactors and GDPs can often be increased by use of commercial observation satellites, i.e. without intrusive, on-site inspections.

Capabilities of the new generation of commecial satellites

Starting in 1999, a new generation of commercial satellites has been launched with 1-meter spatial resolution at visible wavelengths (see Table 3). Although still an order of magnitude less capable than military imaging satellites[3], the resolutions of these new satellites are an order of magnitude better than the 10-30 meter resolution of previous-generation commercial observation satellites such as France's SPOT and the U.S. Landsat 4 and 5 whose capabilities for treaty verification have already been examined in previous studies.[4] Although we have not yet had the opportunity to analyze carefully images of nuclear facilities taken by the new high-resolution commercial satellites, a large number of older images of such facilities with comparable resolution have become available as a result of the declassification of "Corona" panchromatic satellite images taken by U.S. KH-4 intelligence satellites during the period 1967-72.[5] The spatial resolutions of these images – especially towards the end of that period -- are comparable to those of the new high-resolution commercial satellites.[6]

Table 3: Current and planned commercial satellites with high-resolution at visible and near-infrared (VNIR) wavelengths

Satellite System	Owning Country	Launch Date	Res.[a](m) Pan/Mul[b]	Revisit Time (days)	Swath Width (km)	Max. View Angle (degrees)	Orbit Altitude (km)
KVR-1000	Russia	1987	5	14	-	-	200
Iris-1C 1D	India	1995,7	5.8	5	70	26	817
Spin-2	Russia	1990s	2	-	2,10,40	-	220
IKONOS	U.S.	9.24.99	1/4	1-4	11	26	681
QuickBird	U.S.	2000	1/4	1-5	27	30	600
OrbView	U.S.	2000	1, 2/4	3	8	45	460
EROS-A	Israel	2000	2	3	14	45	480
EROS-B	Israel	2001	1	1	20	45	600

a. Instantaneous field of view of sensor pixel.
b. Panchromatic/multispectral. A panchromatic sensor takes a single image of an observed object by collecting light over a wide wavelength band. It is usually referred to as "black and white" mode. A multispectral sensor takes a separate image of an observed object in each narrow wavelength band of light it is designed to detect.

Thermal infrared (TIR)

Objects with temperatures below 100°C emit dominantly at wavelengths longer than 8μm. Satellite TIR images are therefore obtained through the atmosphere's 8-14 μm transmission "window." These wavelengths are 20 times longer than visible wavelengths, which center around 0.5 μm. In a diffraction-limited system, an aperture 20 times larger is therefore needed to achieve the same resolution. To achieve the same resolution from a given altitude would therefore require an aperture 20 times larger.

Measuring absolute temperatures accurately with TIR requires corrections for atmospheric transmission. The most useful information for verification purposes, however, is usually the *difference* between the temperature of an object of interest and its surroundings. We will therefore refer to the "temperature sensitivity" of a TIR image as its ability to resolve temperature differences. Lansat-5 and –7 have spatial resolutions in the TIR region of 120m and 60m respectively, and temperature sensitivities of about 0.5-1°K. ASTER, a satellite with TIR spatial resolution of 90m and temperature sensitivity of 0.2°K at 300°K was launched in December 1999 (see Table 4).

Table 4: Satellites with TIR (8 -14 μm) Sensors

Satellite	Country	Launch date	TIR Resol. (m)	Temp. Sensitivity	Altitude (km)	Swath width (km)	Revisit Time (days)
Landsat-5	USA	1984	120	0.5-1	705	185	16
Landsat-7	USA	4.15.99	60	0.5-1	705	185	16
ASTER	USA/Japan	12.28.99	90	0.2	705	60	16

Monitoring the operating status of reactors and GDPs at visible wavelengths

While a reactor is operating and for a time after shutdown, removal of heat from the reactor core is essential to prevent meltdown of its fuel. A variety of cooling systems for dissipating the waste heat into the environment have been used, including cooling towers, cooling ponds and once-through or condenser cooling with river or seawater.[7] Table 1 lists the cooling systems of plutonium-production reactors, as far as we have been able to determine them.

GDPs produce so much waste heat that they too must have such cooling systems. Producing the 25 kilograms, or what the IAEA describes as a "significant [i.e. weapons] quantity" of weapon-grade (90% U^{235}) uranium in a year, would require an average of about 1.5 megawatts of electric power.[8] More than 90 percent of the electrical energy is converted into compression heat which is dissipated by the plant cooling towers or into a local water body via cooling water (see Figure 1).

Cooling towers

Cooling towers are classified according to the method used for heat transfer to the air and the method utilized to create air movement through the tower.[9] Most cooling towers are "wet," which means that their primary heat-removal mechanism is through the vaporization of water on heat-exchange surfaces. In a dry tower, heat is transferred to air without the addition of water vapor. However, a significantly larger cooling tower is required for a given cooling capacity.[10]

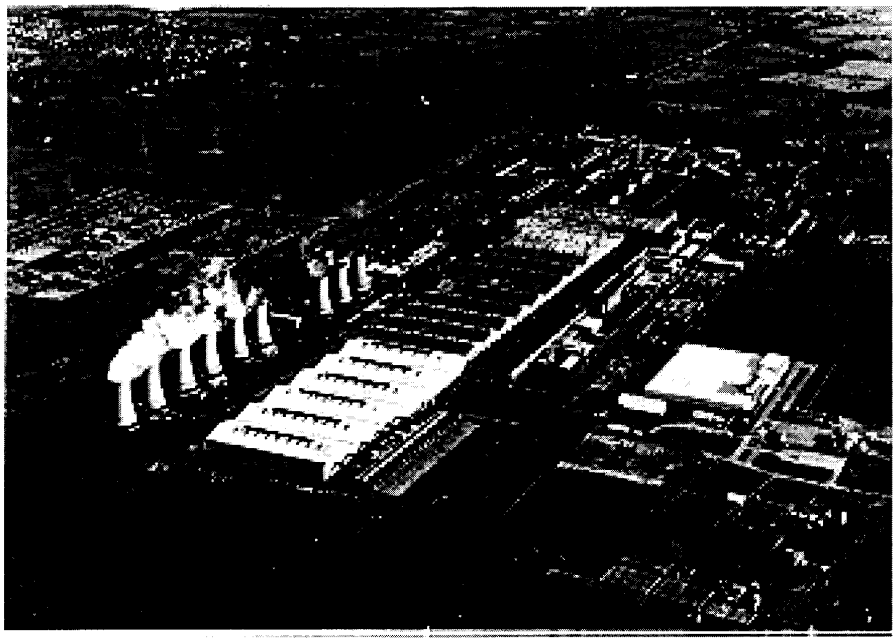

Figure 1: Aerial view of Britain's Capenhurst uranium-enrichment complex when the GDP (the long building running across the center) was operating. Its 11 natural-draft cooling towers are visible. The square flat building to the right contains the first module of the CEP plant. Source: Allan S. Krass et al, Uranium Enrichment and Nuclear Weapons Proliferation (Taylor & Francis, 1983).

In both cases, air circulation through the tower results, at least in part, from the buoyancy of the heated air, which creates a chimney effect. Towers that rely solely on this buoyancy effect are classified as "natural-draft" towers. When large fans are used to increase the air flow through the tower, the tower is classified as a "mechanical-draft" tower. It will be seen from table 1 that most production reactors with cooling towers use wet-type, natural-draft, hyperbolic cooling towers.[11]

A group of such natural-draft towers associated with four of Britain's formerly dual-purpose production reactors is shown in Figure 2. It will be seen

that they are very large: several tens of meters in height and more than 10 meters in diameter at the top. It is easy to identify such a large structure using 1-m resolution satellite images.

When a cooling tower is operating, a water-vapor plume will ordinarily be seen emerging from its top. The air is almost saturated after it passes through wet packing at the base of the tower and cools as it rises through the tower. It is therefore slightly supersaturated when it emerges. Since the diameter of the tower exit is on the order of ten meters, even a short plume will be easy to detect with a 1-m resolution satellite image. Downwind from the tower the air mixes with cooler ambient air resulting in a mix which is more supersaturated. How far downwind the mix remains supersaturated depends upon the relative humidity of the ambient air (see Appendix A).

Figure 3, an image taken by a CORONA satellite on 15 Sept. 1971,[12] includes the cooling towers associated with two of the five plutonium-production reactors then operating at the Siberian Chemical Combine (in Seversk, then called Tomsk-7). The six towers at the upper left and the eight towers at the bottom right are, in all likelihood, associated with the EI-2 (1200 MWt) and ADE-3 (1900 MWt) reactors respectively and would therefore have a cooling capacity of about 200-250 MWt each.[13] The diameters of the tower tops are about 30 meters.[14] The ground resolution in this panchromatic image is about 1.8m.[15] The physical structures of the cooling towers, and the vapor plumes at some of their tops can be seen clearly. The clarity of a commercial satellite image with a 1-m pixel resolution would be comparable (see Figure 12B). It is therefore clear that a 1-m-resolution commercial satellite could detect vapor plumes from operating cooling towers.[16]

Since it requires at least several weeks of irradiation to produce a practical concentration of plutonium in reactor fuel, the several-day revisit time of current commercial satellites should be adequate for detection of operation. Much shorter revisit times will, of course, be possible when there is a constellation of such satellites. This could make it possible to monitor the frequency of shutdown of power reactors equipped with cooling towers. Since the fuel in power reactors is irradiated to much higher burnups than in production reactors which produce weapon-grade plutonium, frequent shutdowns would raise suspicion.[17]

It can be seen from table 2 that most GDPs other than those in Russia have wet cooling towers. U.S. GDPs have mechanical-draft cooling towers but their discharges are also usually saturated, resulting in visible plumes downwind.

The individual openings at the tops of mechanical cooling towers are gen-

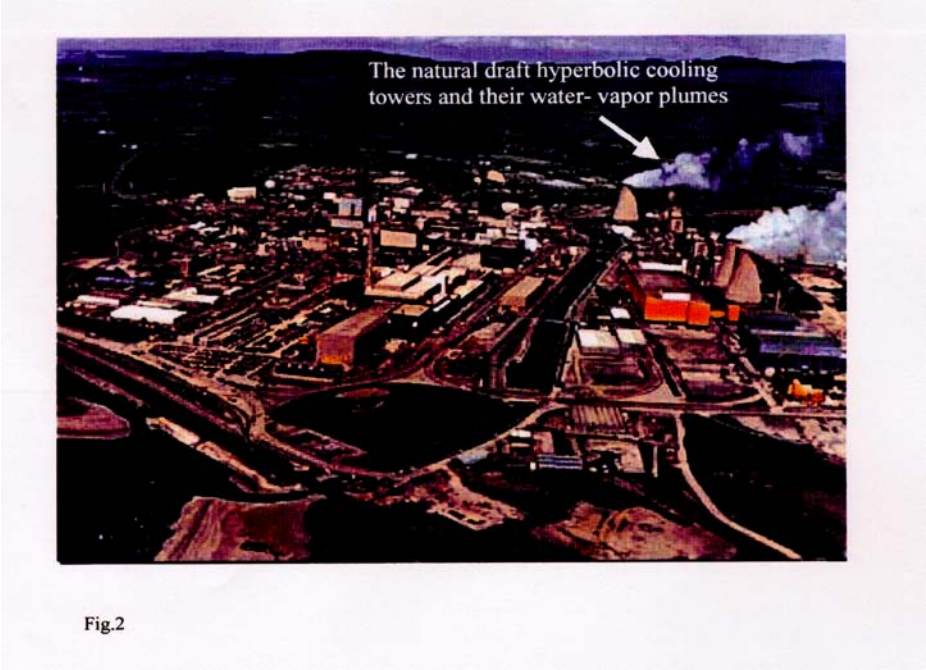

Figure 2: The four 50 MWe Calderhall Magnox reactors at Sellafield, U.K. Note the four huge natural draft hyperbolic cooling towers and their water-vapor plumes. The reactors, originally "dual purpose," producing electricity as well as plutonium and tritium for weapons, now no longer produce plutonium for weapons. Source:http://www.fas.org/nuke/guide/uk/facilit/; http://www.insc.anl.gov/nre/.

erally smaller than those at the tops of natural draft cooling towers. But high-capacity mechanical cooling-tower buildings have many cells. In such cases, the combined area of all the openings – and that of the combined plume they produce, will be quite large. Figure 4b shows a Landsat-5 image in the visible band of the U.S. Portsmouth GDP. Even though the spatial resolution is only 30-m, vapor plumes from the cooling towers can be clearly seen. The plumes would be much clearer in a 1-m-resolution satellite image.

Because of its large inventory of in-process UF_6, the time required for a GDP producing “weapon-grade” (90% U^{235}) uranium to reach equilibrium is

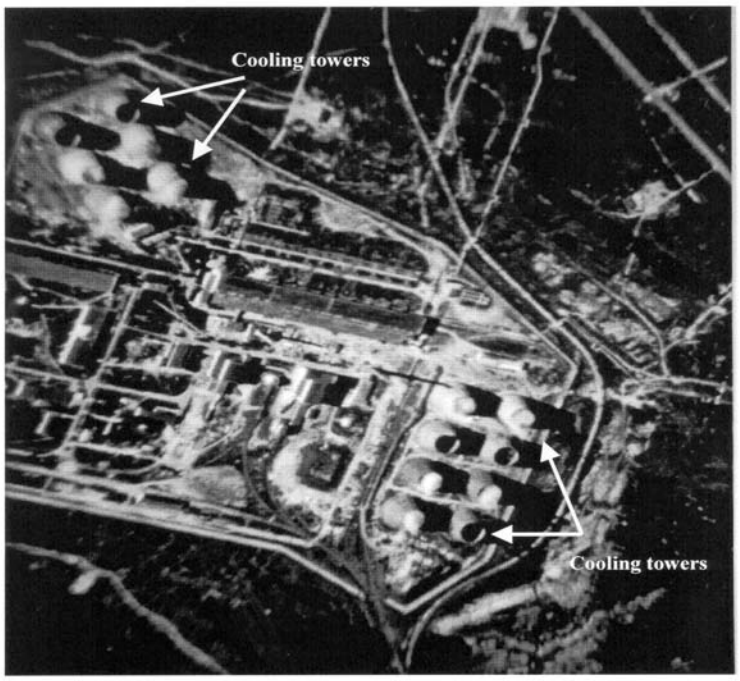

Fig.3

Figure 3: Declassified U.S. satellite image of cooling towers associated with two Russian plutonium-production reactors at Seversk (formerly Tomsk-7). Note that the operating cooling towers have water vapor clouds within them and are also somewhat obscured by thinner plumes above. (Corona mission 1115-1, Sept. 15, 1971, KH-4B with 1.8 m resolution at nadir).

about two to three months.[18] A satellite revisit time of several days should therefore be adequate for detection of GDP operation.

Figure 5 shows a Corona image of the site of Israel's Dimona plutonium-production reactor. The reactor is equipped with a mechanical-draft cooling tower with two vents. The power of the reactor has been estimated as on the order of 70 MWt. However, the dry desert air at the production site could make it possible to minimize the presence of a condensation plume coming out of the tower. Verifying the shutdown of this reactor using commercial imaging satellites is therefore likely to be difficult. The released IKONOS image over

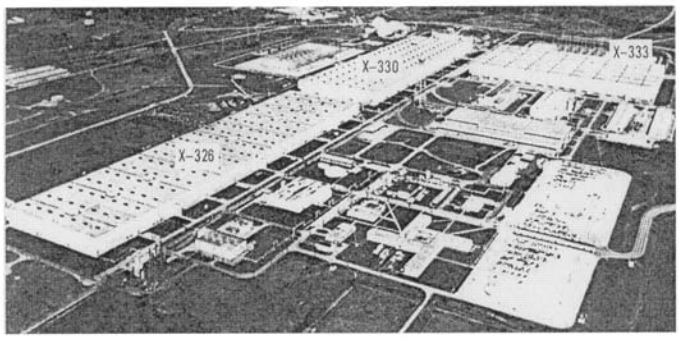

Fig.4a

Figure 4a: Portsmouth GDP process buildings (X-326, X-330 and X-333). Note the roof vents for discharging hot air. Source: AEC Gaseous Diffusion Plant Operations, ORO-684, Jan.1972, U.S. Atomic Energy Commision, Washington, D.C.

the Pakistan Khushab reactor also shows clearly the reactor has a mechanical–draft cooling tower.[19] One can barely see vapor plumes over some vents in the images acquired on February 2000, confirming that the reactor was operating. From the tower's size, it appears that the reactor power is comparable to that of the Dimona reactor.

A reduction of the humidity in the effluent air by on the order of 10 percent would eliminate the vapor plume. This could be accomplished by mixing ambient air with the saturated air inside the cooling tower (see Figure A-1). Unless the ambient humidity were very low, however, the penalty would be a

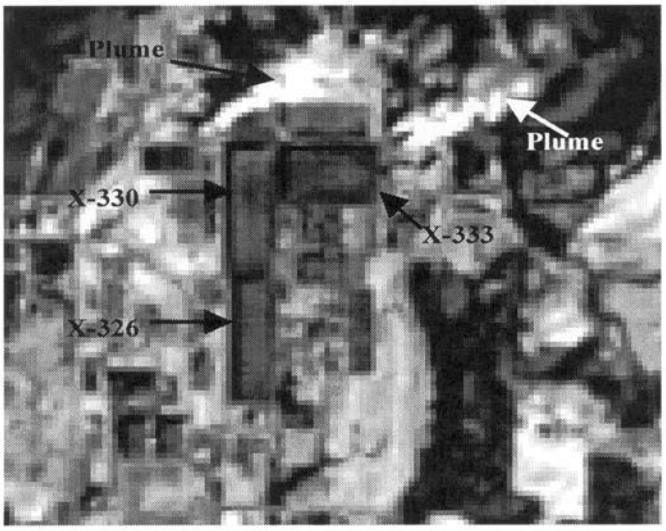

Fig.4b

Figure 4b: Landsat-5 visible image taken Feb.16, 1991. The plumes from the mechanical cooling towers at the northwest and northeast corners of the process buildings are clearly visible in the images. The images in figures 4b, c and d were provided by Adam Bernstein, Monitoring Large Enrichment Plants Using Thermal Imagery from Commercial Satellites: A Case Study (Sandia National Laboratories report SAND 2000-8671, 2000), 15.

large reduction in the cooling capability of the tower.

Holding ponds

Reactors with "once-through" cooling systems often have a holding pond where river water is stored before being treated and pumped through the reactor. These holding ponds can also be used for emergency cooling water if the pumps from the river fail. Figure 6a shows a triplet of holding ponds in front of the L-reactor at the U.S. Savannah River Site. A dried-up holding pond would be a good indicator that the reactor had been shut down. This

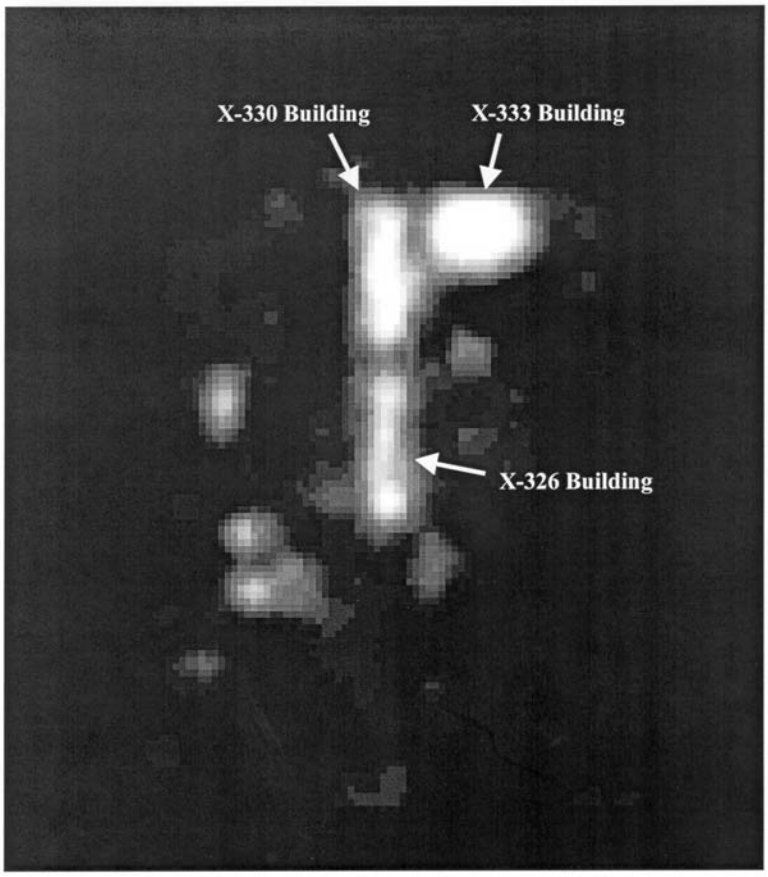

Figure 4c: Landsat-5 TIR image taken March 12, 1994. The hot roofs of buildings X-333, X-330 and X-326 are clearly visible.

could be detected in an 1-m resolution image through the change in reflectivity of the pond area. This is illustrated in Figure 6b, a 1969 CORONA KH-4B photograph of three huge storage ponds near the Jiuquan nuclear complex in China. The two dark ponds on the left appear to contain water while the one on the right appears dry.

Only in dry climates such as that in the Jinquan area will holding ponds dry out, however, when not in use. In a wet area such as the Savannah River site, where rainfall exceeds the rate of evaporation, the pools will remain full unless a drain is opened.

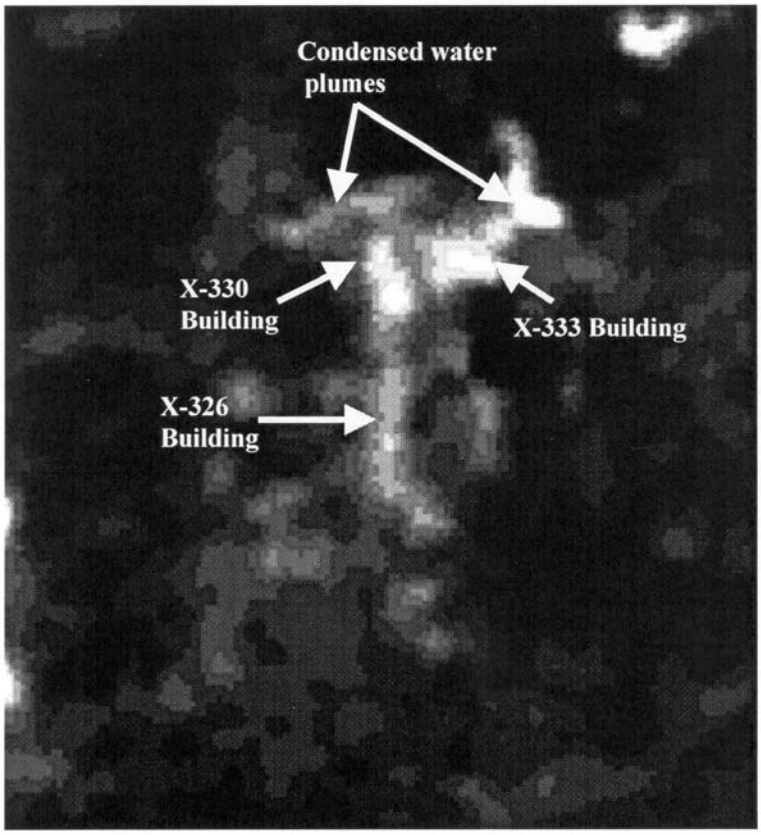

Figure 4d: Landsat-5 TIR image taken Feb. 16, 1991. The roofs of the process buildings are less apparent than in Figure 4c – probably due to the cooling effect of a brisk wind. However, the steam plumes observed to the northeast and northwest of the process buildings in the counterpart visible image in Fig. 4b are apparent in the TIR image as well.

Monitoring the operating status of production reactors and GDPs at thermal-infrared wavelengths

Thermal-infrared (TIR) sensors can detect small temperature differences, but, because of their relatively poor spatial resolution, the objects they detect have to be either very large or hot enough so that they result in above-detection-threshold radiation increases in one or more pixels (see Appendix B).

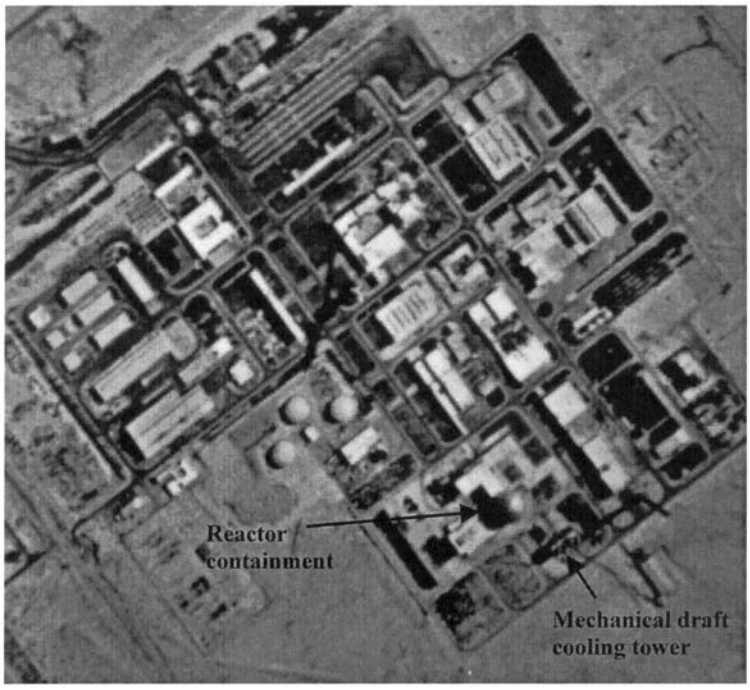

Figure 5: Declassified U.S. Corona Satellite Image of Dimona Nuclear Facilities in Israel. (Mission 1115-2, 29 September 1971, KH-4B system with 1.8 m spatial resolution) Source: http://www.fas.org/irp/imint/4_dim_03.htm.

Cooling towers

Although they have much poorer spatial resolution, TIR sensors, unlike VNIR sensors, can detect the warm plumes of water vapor emerging from cooling towers at night as well as during the day – and also against a snowy background. The plumes are visible in TIR only in the same region where condensed droplets of water vapor make them visible to the eye. This is because water molecules and air molecules in the gas phase radiate only at their characteristic molecular wavelengths, which are generally reabsorbed by the same

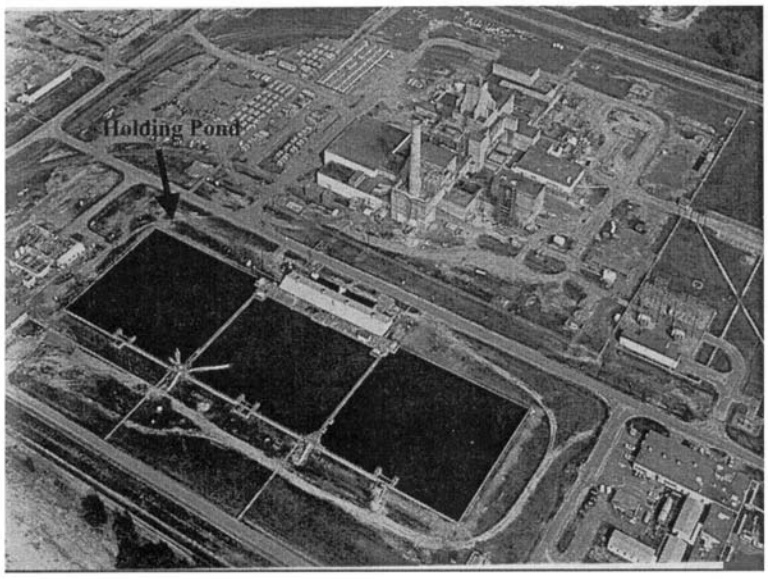

Figure 6a: Cooling water holding ponds in front of the L-Reactor at Savannah River Site, U.S. Source: Thomas B. Cochran, William M. Arkin, Robert S. Norris and Milton M. Hoenig, Nuclear Weapons Databook, Volume III: U.S. Nuclear Warhead Facility Profiles, (Ballinger, 1984).

classes of molecules above in the cooler higher atmosphere before the radiation escapes and is detected by a satellite sensor. Some of the black-body radiation emitted by the droplets in a visible vapor plume, by contrast, is emitted in the atmospheric transmission windows in the 8-14 μm region between the molecular absorption bands and therefore can escape from the atmosphere.

The visible plume from a cooling tower is usually at least few degrees Centigrade warmer than the ambient air. The size of the area it covers depends upon the humidity of the ambient area (see Appendix A). If the size is comparable to the instantaneous field of view (IFOV) of a pixel in the TIR sensor and

Figure 6b: Holding ponds at Jiuquan Nuclear Complex. The three huge ponds near the Jiuquan Reactor are most likely there to hold a backup water supply for the reactor. The darker ponds appear to have water in them. Declassified U.S. Corona Satellite image. Corona Mission 1108-1 on 9 Sept 1969, KH-4B system with 1.8 m resolution.

if it is also warmer than the ground below, the relative temperature difference should easily be detectable by the sensors on Landsat-5,- 7 and ASTER, which have relative temperature resolutions of better than 1 $^{\circ}$C (see Table 4). Indeed, the steam plumes from the cooling towers of the Portsmouth GDP, observed to the northeast and northwest of the process buildings at visible wavelengths in Figure 4b are also visible in the associated TIR image (Figure 4d) as well.[20]

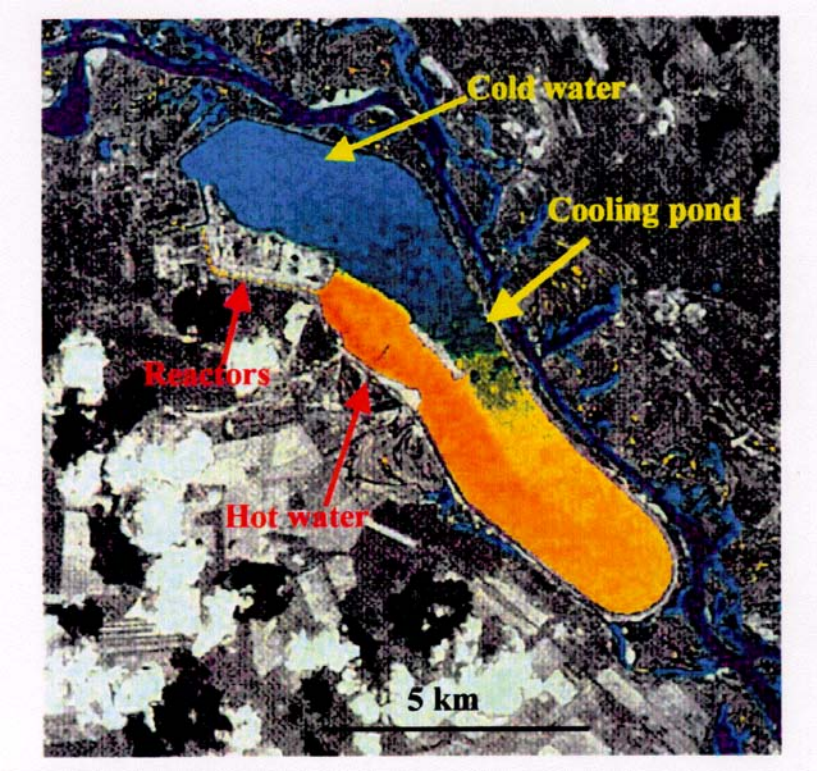

Figure 7a: Landsat-5 TIR image of Chernobyl Nuclear Reactor Site, Ukranine. This image was taken on 22 April 1986 when the reactors were in normal operation.

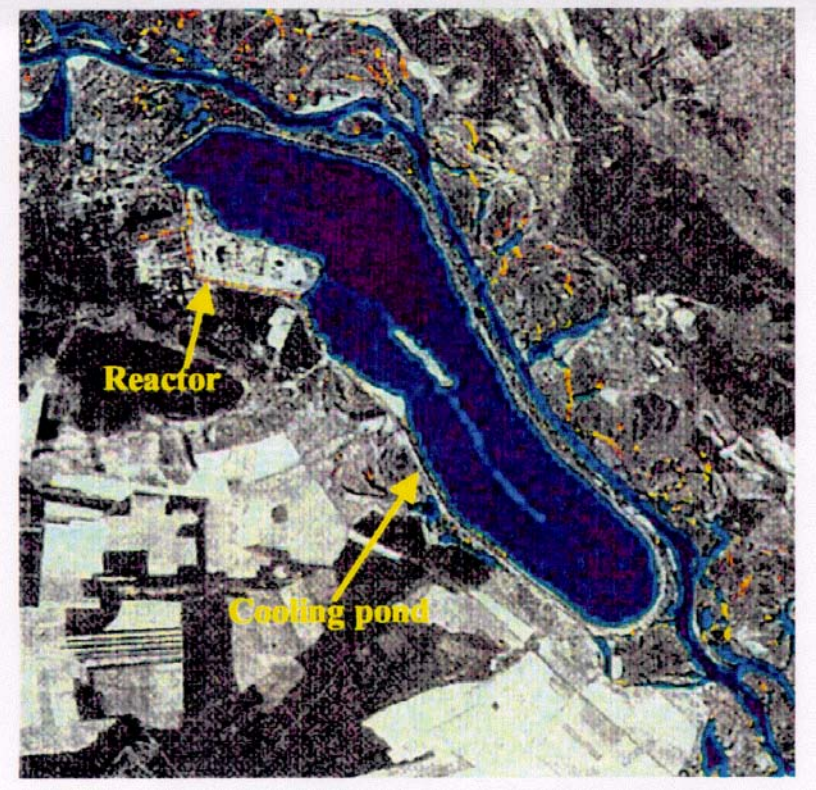

Figure 7b: Landsat-5 TIR image taken on 8 May 1986 (after the April 26 accident, when operation was suspended).

Cooling ponds, rivers, estuaries, etc

Cooling ponds are water bodies in which cooling water dissipates its heat into the atmosphere through radiation, convection, conduction and evaporation. Because of their low heat transfer rates per unit area, they require a large surface area. In Appendix C we estimate the required area per unit of power as

$$A/P = (1nr)/[K\Delta T] \quad km^2/MWth \qquad (1)$$

Here K is the heat transfer coefficient from the water to air and (by TIR radiation) to space, typically in the range 20-40 $(MW)/(km^2 \cdot °C)$, ΔT is the difference between the coolant discharge temperature (T_d) and intake temperature (T_i), and

$$r = (T_d - T_e)/(T_i - T_e)$$

where T_e is the equilibrium temperature the cooling pond surface would have if the power plant were not operating.

Consider as an example the case of the cooling pond for the Chernobyl Nuclear Reactor Site (Figure 7). Assume K = 30 $Watts/(m^2 \cdot °C)$, and assume values of 35, 25 and 20 °C for T_d, T_i and T_e respectively. These values give r = 3 and $\Delta T = 10$ °C. Substituting in Eqn. 1 gives A/P = 3.7 km^2/GWth, which is consistent with handbook estimates of 2-8 km^2/GWth.[21]

Before the April 26, 1986 accident, the four reactor units on the Chernobyl site sometimes operated simultaneously. The electricity output for each unit was about 1 GW electric and the conversion efficiency of heat into electricity was about 33 percent. The cooling pond was therefore designed to dissipate up to about 8 GWth. For the values of K, r and $T_d - T_i$ that we have assumed, the area of the cooling pond calculated from Eq.(1) is about 20 km^2, which is roughly consistent with Figure 7, obtained with the Landsat TIR imager which shows the surface temperature distribution in the cooling pond before and after the April 26, 1986 accident.[22]

Figure 8 shows two Landsat-5 thermal images of the "Mayak" plutonium and tritium production complex at Ozersk (Chelyabinsk-65) in the Urals, acquired by Bhupendra Jasani et al.[23] In both images, a plume of warm water can be clearly seen extending north for a considerable distance along the eastern fringes of Lake Kyzyltash. The surface temperature of the water within the 1987 plume is a maximum of 10 °C warmer than that of the bulk of water in the lake. In the 1993 thermal image, the warm plume is larger and a maximum of 15 °C warmer than the bulk of the water. The plume is presumably associated with the tritium-production reactors since all five plutonium-production reactors at this site had reportedly been shut down by the end of 1990 (see Table 1).

Figure 9 shows a TIR thermal pattern obtained from an aircraft flying at an altitude of 1.2 km. It shows the hot-water discharges from the C and L reactors at the U.S. Savannah River Site flowing into a swampy area next to the Savannah River.[24] The reactors operated at powers greater than 2.5 GWth. The streams of hot water are about 4 km long and cover an area of

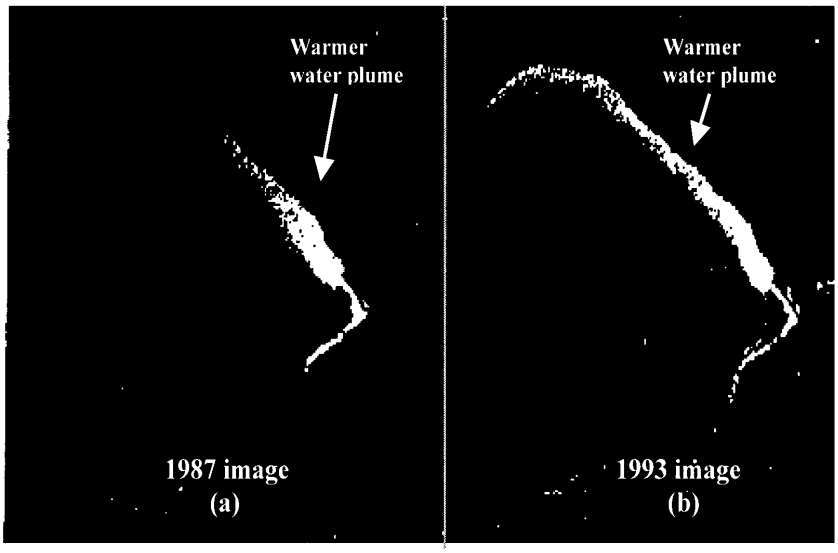

Figure 8: Landsat-5 TIR images of hot-water discharges into Lake Kyzyltash from the Ozersk plutonium and tritium production complex: a) August 1, 1987; b) May 13, 1993.

more than 0.5 km^2 at temperatures at least 5 $^{\circ}K$ higher than that of the river. The Hanford reactors discharge their hot water into the Columbia River. India's Dhvrua and Cirus research reactors at Trombay discharge their hot water into a bay (see Figure 10).

As long as cooling water is discharged into surface waters, an area of elevated temperatures around the discharge point should be detectable using satellite-borne TIR sensors. However, in theory at least, a discharge could be concealed by releasing it through a long pipe with many holes along its length laid in deep water so that a mix results with a temperature which is not

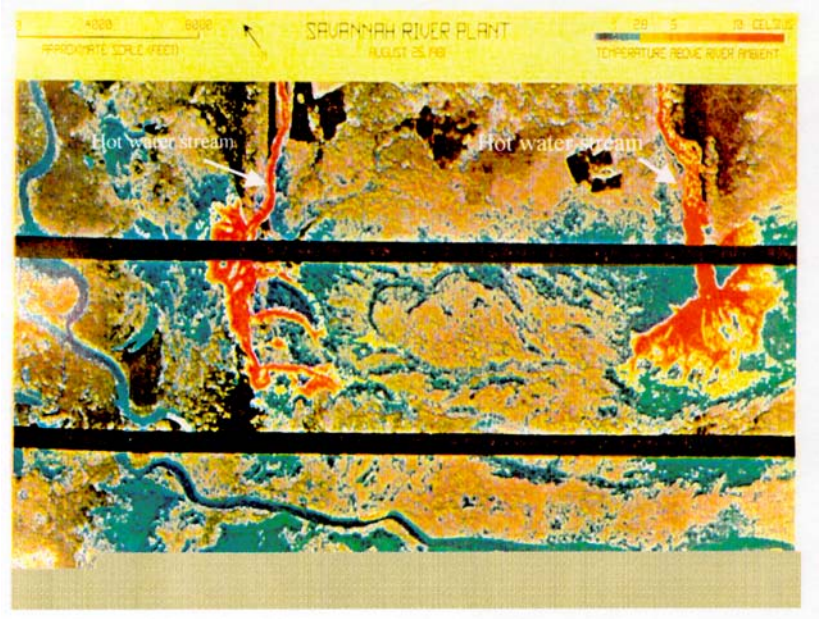

Figure 9: TIR image of hot water discharged into swamps from two plutonium production reactors at the U.S. Savannah River Site.

detectably warmer than that of the surface waters above. For a 15 °C temperature rise, the volume of a discharge carrying away 1 GWth would be 16 m^3/sec. To bring that temperature down to the 0.2 °C temperature rise detectable by ASTER would require dilution by a factor of 75 to a volume of 1200 m^3/sec. For comparison, the flow past Krasnoyarsk of the Yenesei River, the largest River in Russia, is at least some thousands of m^3/sec.[25] The three underground nuclear reactors that discharged into the river nearby had a combined thermal power of up to 6 GW so, with perfect mixing, it might be possible to conceal their output from ASTER. A reactor with a capacity of only 0.03

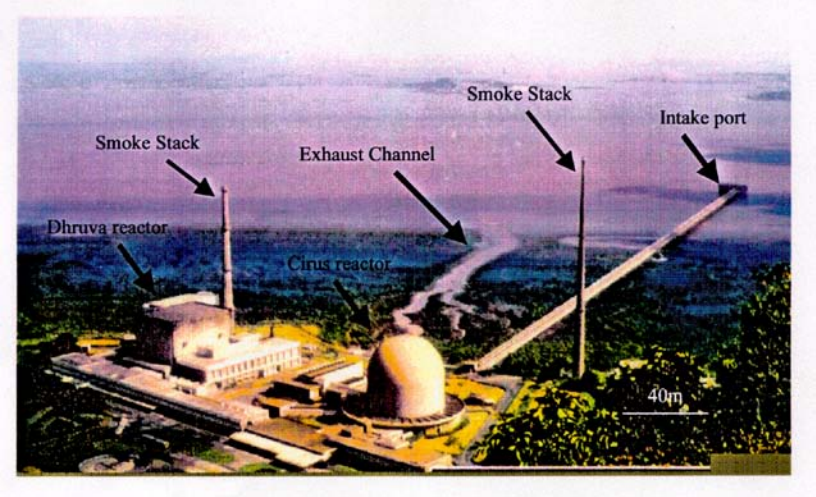

Figure 10: Cooling arrangements for India's Cirus and Dhruva " isotope-production" reactors at Trombay. The reactors use natural-uranium fuel and heavy-water moderator. The 40 MWth Cirus reactor began operation in 1960; The 100 MWth Dhruva reactor started in August 1985. Both reactors produce plutonium for India's nuclear weapons and operate without IAEA safeguards. Cooling water from the bay is drawn through the long structure. The discharged water flows back into the bay in the stream. The lighter discharge water can be seen mixing into the darker water of the bay. [Source: Image acquired by Space Imaging's IKONOS Satellite, February 27, 2000.]

GWth could produce one "significant quantity" of plutonium per year. Many rivers have enough flow to conceal the heated cooling water from such a small reactor.

Detection of the elevated temperature of the roof of the process building of an operating GDP

The lowest UF_6 temperature in a GDP must be safely above the UF_6 condensation or freezing temperature (see phase diagram of UF_6 in Figure 11).[26] The

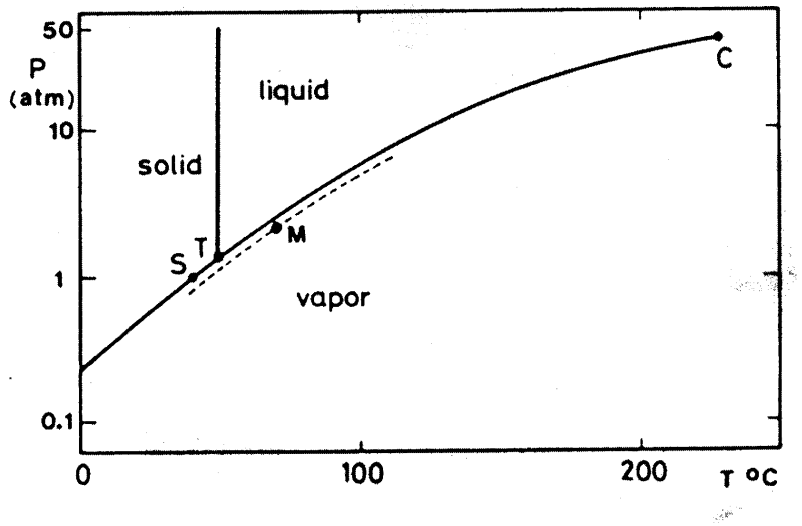

Figure 11: Phase diagram of UF_6. At the triple (T) and critical (C) points, temperature and pressure are (64.05 °C, 1.50 atm.) and (230.0 °C, 45.5 atm.) respectively. The sublimation temperature (at point S) at 1 atmosphere is 56.5 °C. The dashed line with the point M on it denotes operation points safe from UF_6 condensation hazards. Source: S. Villani, "Uranium Enrichment," in Topics in Applied Physics 35 (Springer-Verlag, 1979).

operating temperature for the process gas is typically higher than 70 °C (158 °F). Consequently, the air temperature in the areas containing the compressors are typically much higher than the outdoor temperature.[27] In U.S. plants these areas are in the upper floor of the process buildings. To maintain cooler temperatures in the working areas below, outside air is sucked into the first floor and exhausted through the roof. The vents in the tops of the Portsmouth enrichment process buildings are visible in Figure 4a. Because of the large areas of GDP processing buildings, the elevated temperatures of their roofs are detectable using commercial-satellite TIR images.

Case study: the U.S. Portsmouth GDP[28]

The Portsmouth GDP in southern Ohio has been operating since 1954. In 1993 the plant ceased production of HEU. However, it continues to produce LEU for nuclear power reactors.

The enrichment "cascade" is contained in three large, two-story buildings identified as X-333, X-330 and X-326 (see Table 2 and Figure 4a). In all three buildings the process-gas equipment and associated valves and piping are located on the upper floors. Each process building has its own cooling system that dissipates the waste heat to the environment through evaporative cooling towers. The GDP consumes about 2260 MWe when operating at its full separative capacity of about 8.3 million SWU/yr.[29] Typically the plant draws about 1000 MWe. This corresponds to a typical power consumption per unit area of the process buildings of about 2.6 kW/m^2.

The Portsmouth GDP process buildings are so huge that each can cover the IFOV of several Landsat-5 pixels, and they are so hot that their temperature elevation should be detectable when the compressors inside are operating. For a thermal emissivity of unity, the threshold sensitivities of the TIR detectors are 0.5-1 °C for Landsat-5, -7 and 0.2 °C for ASTER – corresponding to radiation flux increases of 3-6 and 1Watt/m^2 respectively – about one thousandth of the power consumption of the plant.

During the day, the temperature of the roof of the GDP might be different from that of the surrounding area due to its differing solar absorption, and during the night it might cool down at a different rate because of its different thermal inertia and exposure to the wind. Assurance of detection of operation is therefore likely to require a larger increase in the roofs' temperatures than the threshold value estimated above.

In a morning (~9:45 AM local time) TIR image acquired by Landsat-5 in March 1994 (Figure 4c), the roofs of the process buildings are visibly radiating much more strongly than the background. In an earlier image taken in February 1991(~9:45 AM local time) (Figure 4d), the buildings are visible but less clear in the TIR – perhaps due to the cooling effect of a relatively stiff winter wind.[30] The clearly visible (at both visible and TIR wavelengths) warm vapor plumes coming out of some of the mechanical-draft cooling towers indicate that the plant was operating. Based on these results, we expect that the TIR images obtained with ASTER would show the warmth of the processing buildings under virtually all conditions when the GDP is operating.

Case study: China's Lanzhou GDP

The Lanzhou GDP (plant 504) located on the bank of the Yellow River near Lanzhou in Gansu Province was China's first source of weapon-grade ura-

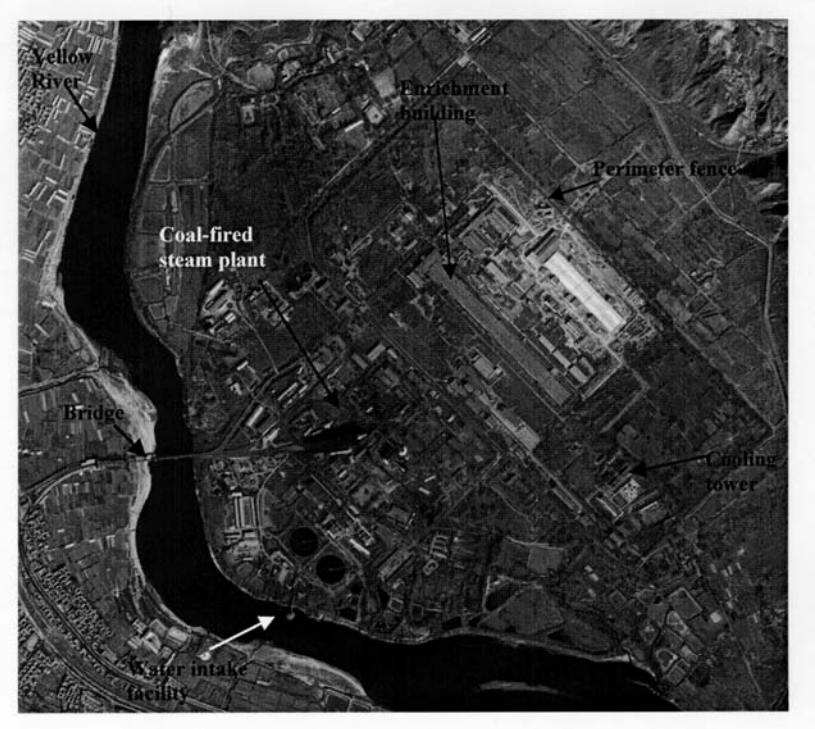

Figure 12a: A satellite image of the region around the uranium-enrichment GDP near Lanzhou, China. The dimensions of the long leg of the enrichment building are approximately 600 m by 60 m. This one meter resolution black-and-white image was taken at approximately 10:30 AM, February 5, 2000 by Space Imaging's IKONOS satellite. Credit: "spaceimaging.com."

nium. It began operation in mid-January 1964. Published estimates put its initial capacity at 10,000-50,000, increased later to about 300,000 kg-SWU per year.[31]

Figures 12 show an IKONOS satellite image of the Lanzhou GDP taken on February 5, 2000. We estimate that the enrichment building is about 600 m long and 60m wide. At its final capacity, for a specific energy consumption of 2.5 MWh/kg-SWU, the power consumption of the plant would be 86 MWe or about 2.4 kWt/m^2.

The 60-m width of the Lanzhou plant means that it cannot completely fill

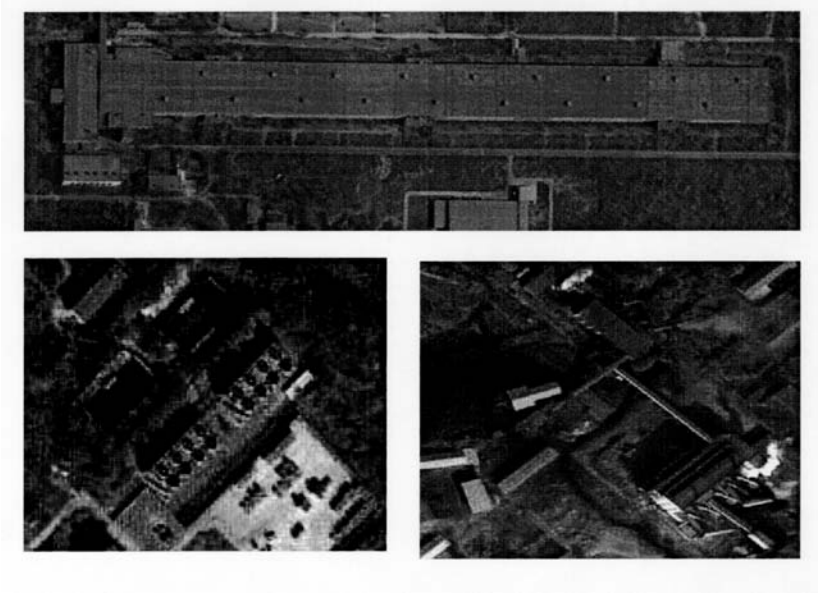

Figure 12b: Close-ups of portions of the Lanzhou image shown in Fig. 12a. The top image is of the building containing the enrichment "cascade" (note the hot-air vents on the roof). The bottom-left image is of the associated bank of mechanical cooling towers (two rows of 8). The absence of vapor plumes indicates that the plant is not operating. The bottom-right image is of a coal-fired plant. Part of the coal pile appears as a black area in the middle left and the long narrow structures cover converyor belts carrying the coal to the boilers. The vapor plumes may be from unresolved mechanical cooling towers associated with the coal-fired plant. Credit: "spaceimaging.com."

the IFOV of Landsat 5 or ASTER pixels (120 and 90 m wide respectively). This increases the incremental TIR energy flux required to meet the threshold conditions for detection by a factor on the order of 2-4 for Landsat 5, 1-2 for Landsat 7, and 1.5-3 for ASTER, depending upon the degree of match of the IFOV of their pixels with the plant width (see Appendix B).

A Landsat-5 thermal image of Lanzhou GDP was acquired on Feb.3, 1989. The process building was not detectable at thermal wavelengths. It is possible that the plant was not operating.[32] It is also possible, however, that it was operating and the pixel-average radiated power was below the discrimination

threshold of the Landsat-5 TIR detector. In either case, we would expect the TIRs of Landsat-7 and ASTER to be able to detect its operation under most ambient conditions if the insulating properties of the roof are comparable to those of the Portsmouth GDP.

Similar analyses could be carried out for the UK's Capenhurst GDP (100-150tSWU/yr) and France's Pierrelatte GDP(400-600tSWU/yr).

Case Study: Pakistan's Kahuta Centrifuge Enrichment Plant

On-site verification measures will be required to verify that HEU is not being produced in operating uranium enrichment plants and we expect large centrifuge enrichment plants (CEPs) to continue to operate to produce LEU for nuclear power plants under a moratorium or cutoff of the production of fissile material for weapons.

Small uneconomic CEPs, such as that operated by Pakistan at Kahuta, might be shut down. Because of their small size and relatively low energy intensity, however, such plants do not require special cooling systems such as cooling towers.

The electrical consumption of a gas centrifuge facility is much less than that of a GDP. The specific energy consumption of a CEP typically ranges from 100 to 300 kWh/kg SWU, roughly a factor of 10 smaller than for a GDP.[33] Chilled air is typically used to cool various systems in the plant, with the final heat rejection to the atmosphere being through roof-mounted air-cooled radiators or mechanical cooling towers.

Beginning in the mid-1980s, Pakistan is believed to have produced weapon-grade uranium at the Kahuta CEP in sufficient quantity for nuclear weapons using centrifuges based on URENCO designs and is believed to have a production capacity of about 9000-15,000 kg-SWU/yr.[34]

The size of the Kahuta CEP processing building can be estimated through scaling from that of the first Almelo plant located Netherlands. This demonstration CEP plant, which became operational in 1976, had a capacity of 200,000 kg-SWU/yr. Its overall area was about 120x120 (= 14,000 m^2).[35] Assuming 100-300 kWh/(kg-SWU), this CEP would dissipate 100 - 500 kWt of heat or 150-460 Watts/m^2. For comparison, an ordinary U.S. office building consumes an average of about 70 Watts/m^2.[36]

The size of the original Almelo plant was just about equal to the IFOV of a pixel. Landsat-5 TIR images of this plant and its nearby sister plant in Gronau, Germany were acquired by Jasani et al on July 19, 1992. No convincing signature was measured in the TIR. It was concluded that it was possible that at the time neither of the plants was operating or, more likely, the temperature increase of the plant roof was too low to be detected.[37] Perhaps a

more sensitive TIR imager, such as that on ASTER, might be able to detect the temperature increase. However, detection of such a low signal would be complicated by wind cooling, etc.

Scaling from the Almelo plant, the Kahuta centrifuges could be fit into buildings with an area of 650-1100 m^2. These areas are 5-10% of the IFOV of Landsat 5, 18-36% of that of Landsat 7 and 8-16% of that of ASTER. Therefore, in order to detect the heat from the roof of Kahuta, the spatial resolution of TIRs would have to be improved correspondingly. This should be feasible. If the optics for a 1-m resolution satellite were coupled with a TIR detector, for example, the TIR spatial resolution would be about 20 m. Still, a signal from one pixel would carry far less conviction than the actual images obtained of the Portsmouth GDP. The fact that it may be possible to start and stop low in-process-inventory CEPs in times short in comparison with the revisit times of a single satellite would be an additional complication.

CONCLUSIONS

In summary:

- 1-m resolution satellite imagery can detect the water-vapor plumes from cooling towers associated with large production reactors and GDPs. It appears that, a fair fraction of the time, TIR sensors can as well. In very dry desert air the plumes will be very short.
- As previous authors have shown, for reactors with cooling ponds or once-through cooling systems, TIR imagery can detect the warm-water plume discharged into the receiving body of water. For discharge into a river with a sufficient flow, the plume could be made invisible by discharging and diluting it below the surface.
- The elevated temperatures of the roofs of very large operating GDPs are detectable with existing civilian satellite TIR imagers. The TIR sensors of Landsat-7 and ASTER might be able to detect the elevated temperatures of the heated roofs of medium-sized GDPs such as that at Lanzhou but that on Landsat-5 probably cannot. It does not seem possible to monitor the operation of a small CEP, such as Pakistan's Kahuta plant with existing commercial satellite TIR imaging systems.

Thus, the new generation of civilian satellites cannot substitute for on-site verification of an FMCT. They could supplement such inspections, however, and, prior to an FMCT coming into force, could increase confidence in production-moratorium declarations when those moratoria result in the shutdown of

production reactors and GDPs. Unlike information obtained by U.S. and Russian observation satellites, the information from commercial satellites could be available to all interested countries and NGOs.

There is a potential concern that a nation could enter into an exclusive arrangement with the operator of a commercial satellite to buy all images of its sensitive sites so as to deny these images to other organizations. Given the number of competing 1-m resolution systems that are being launched, however (see table 3), it appears unlikely that one nation could make such arrangements with all the operators. In the future, an international verification agency could own one or more dedicated observation satellites.[38]

Appendix A. The lengths of vapor plumes from wet cooling towers

In wet cooling towers (both natural-draft and mechanical-draft), the primary cooling mechanism is evaporation. Hot water is dripped through the "packing" in the bottom of the tower as air flows upward through it.[39] Usually the design of the cooling tower results in the air being almost saturated upon leaving the packing. The "wet-bulb" temperature of the entering air (the temperature at which it would be 100% saturated) determines how much water the air is carrying in and the temperature of the exiting air how much is being carried out.

As the air rises, it expands and cools; Condensation of water occurs, resulting in a visible plume almost always being present.[40] After the plume leaves the tower, its buoyancy will lead to a further rise.[41] It will also mix with the ambient air. How far downwind the resulting mixture will remain supersaturated depends upon the saturation level of the ambient air. This is illustrated by a line connecting the points in Figure A-1, a "psychrometric chart"[42] giving the grams of water vapor per m^3 of saturated air as a function of temperature. Point "o" in the figure represents saturated output air leaving a cooling tower at a temperature of about 25 °C. Point "i" represents input or ambient air at about 8 °C and 70 percent saturation. All mixtures of the output and ambient air will lie along the line between these points. The point "c" where this line intersects the saturation curve is usually termed the "critical dilution point." On the line between "o" and "c," the air mixture is supersaturated, condensation will occur and the plume will therefore be visible. From "c" on to "i" the plume becomes undersaturated and the plume will disappear. If the ambient air were already saturated, the visible plume would, in princi-

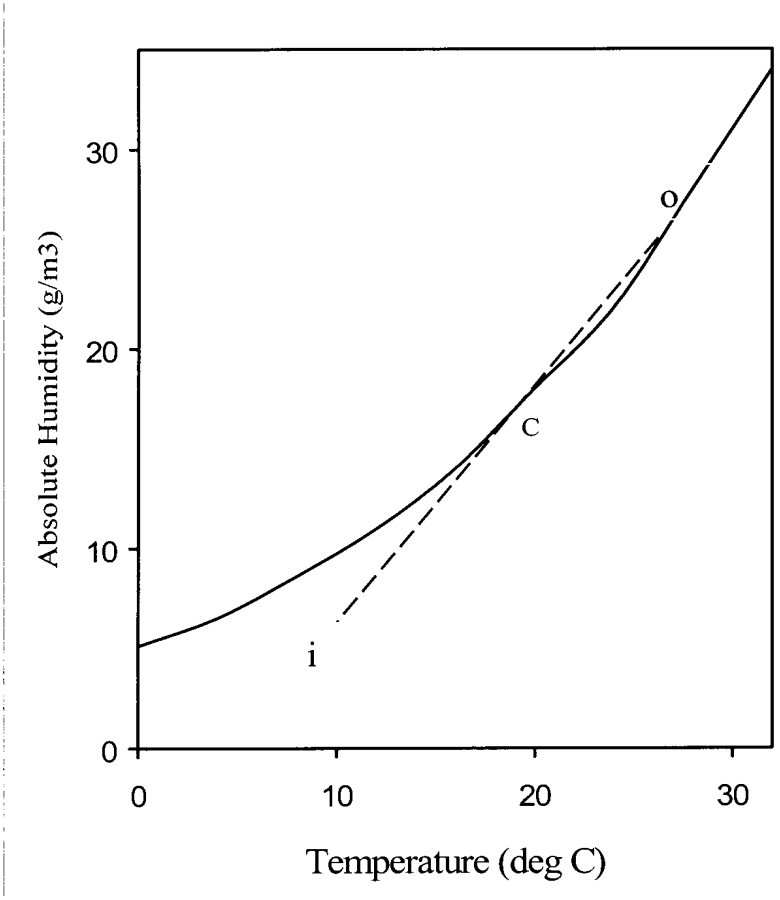

Figure A-1: Simplified psychometric chart showing the saturation humidity of air as a function of temperature. The straight dashed line will be followed by the air in the plume from a cooling tower as saturated air discharged with humidity and temperature corresponding to the point "o" is diluted by ambient air with humidity and temperature corresponding to "i."

ple, extend indefinitely.

Given the linearity of the humidity with dilution, the critical dilution ratio (R_d) for the output air at the critical dilution point is

$$R_d = (T_o - T_i)/(T_c - T_i) \qquad \text{(A-1)}$$

where T_o,T_c and T_i are the temperatures of air at the points “o,” “c,” and i.

Temperature increase and velocity of air discharged from a natural-draft cooling tower

The enthalpy of vaporization of water is about 2.4 Mj/kg and the specific heat of air is 1 $kJ/(kg \cdot °C)$. The flux of energy removal (MWth) per m^2 of exit aperture at the top of the cooling tower is therefore

$$p = j[0.001(T_o - T_i) + 2.4(F_0 - F_i)]\ MWt/m^2 \qquad \text{(A-2)}$$

where and F_i and F_o are the water vapor mass fractions in the incoming and outgoing air, $\Delta T = T_o - T_i$, is the temperature difference between the incoming and outgoing air, and

$$j = \rho_o V_o \qquad \text{(A-3)}$$

is the mass flux of air through the cooling tower aperture in kg/m^2-sec, where ρ_o is the mass density of the exiting air (kg/m^3) and V_o is its velocity (m/sec).

In a natural-draft cooling-tower, the gas exit velocity is determined by the density difference ($\Delta\rho$) between the air inside and outside the cooling tower and by the cooling tower height (h in meters)[43] according to the energy-conservation formula

$$(1/2)\rho_o V_o^2 = K\Delta\rho g h \qquad \text{(A-4)}$$

where g = 9.8 m/sec^2 is the gravitational constant and K is a factor less than one representing the reduction in available potential energy due to dissipative losses in the packing and elsewhere in the tower (typically $K \approx 1/4$).[44] Using the perfect gas law, we have

$$(\Delta\rho)/\rho_o \approx \Delta T/T_i \qquad \text{(A-5)}$$

Eqn. A-4 then becomes

$$V_o^2 \approx (2K)(\Delta T/T_i)gh \qquad \text{(A-6)}$$

or

$$V_o \approx 0.9C_s[\Delta T]^{1/2}\ \text{m/sec} \qquad \text{(A-7)}$$

The scaling factor

$$C_s = [(4K)(h/50)(300/T_i)]^{1/2}$$

equals 1 when K = 1/4, h = 50 m. and T_i = 300 °K.

Substituting (A-3) and (A-7) in (A-2) and approximating $\rho_o \approx 1\ \mathrm{kg/m^3}$ then gives

$$p \approx 0.9 C_s (\Delta T)^{1/2} [0.001 \Delta T + 2.4(F_o - F_i)]\ MWt/m^2 \qquad \text{(A-8)}$$

In A-8, $F_o = F_w^s(T_o)$ and $F_i = f_i F_w^s(T_i)$, where f_i is the fractional saturation of the incoming air and, between 10 and 30 °C,

$$F_w^s(T) \approx [3.7448 + 0.365118\,T - 0.0016594\,T^2 + 0.00047455\,T^3] \times 10^{-3} \qquad \text{(A-9)}$$

is the weight fraction of water carried by saturated air as a function of temperature T in °C.

Figure A-2 shows a plot of p against ΔT for h= 60m , K=1/4, f_i = 0,1, and T_i = 0, 10, 20, 30 °C. For the case of the Tomsk-7 cooling towers, if the flux of energy removal is about 0.3 MWt/m^2,[45] it will be seen that, for T_i = 20 °C and 50 percent humidity ambient air, the temperature increase of the discharged plume is about 14.5 °C. From Eq.(A-7) it will be seen that the velocity of air leaving the towers in this case is about 4m/s.

Plume dispersion

The most common approach to modeling plume mixing assumes Gaussian dispersion. In this case, the increased water concentration along the plume centerline is given by

$$\chi = \frac{Q}{2\pi u \sigma_y \sigma_z}\left\{1 + \exp\left[\left(-\frac{1}{2}\right)\left(\frac{2H}{\sigma_z}\right)^2\right]\right\} \qquad \text{(A-10)}$$

where χ is the increased mass concentration of water (kg/m^3) ; Q is the water-vapor emission rate (kg/sec); and σ_y and σ_z (which are functions of downwind distance, x) are the standard deviations of the plume water concentration in the cross-wind and vertical directions (m) as it drifts downwind.[46] H is the height of the plume centerline (m), which may be a function x if the buoyancy

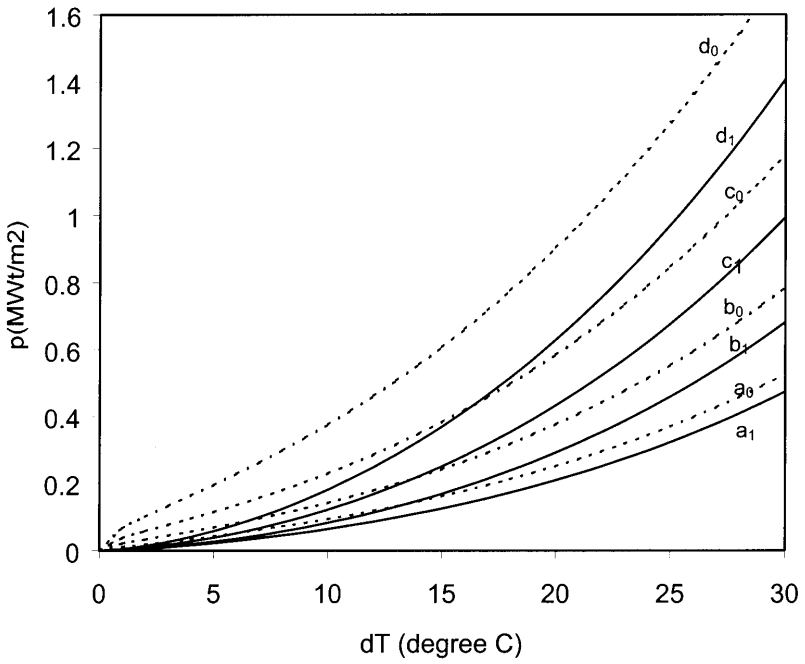

Figure A-2: Cooling tower capacity MWt/m^2 as a function of temperature increase for different ambient air temperatures (T_i) and fractional humidities (f_i). a_0: T_i = 0 ^oC, f_i = 0; a_1: T_i = 0 ^oC, f_i = 1; b_0: T_i = 10 ^oC, f_i = 0; b_1: T_i = 10 ^oC, f_i = 1; c_0: T_i = 20 ^oC, f_i = 0; c_1: T_i = 20 ^oC, f_i = 1; d_0: T_i = 30 ^oC, f_i = 0; d_1: T_i = 30 ^oC, f_i = 1.

of the plume causes it to rise, and u is the mean wind speed (m/sec).

The dispersion parameters, σ_y and σ_z, grow with downwind distance x in a fashion that depends upon stability conditions in the lowest "mixing" layer of the atmosphere. Pasquill has divided these stability conditions into 6 classes, A-F. "A" is the most unstable, for example, in the afternoon of a bright sunny day when the earth is warmer than the atmosphere and therefore generates rising "thermals." "F" is the most stable, e.g. early in the morning after a clear night, when the ground is cooler than the air above. Various modelers have offered empirical functional forms of σ_y and σ_z for each stability category. We

have used the analytic forms given by Green et al.[47]

The initial concentration of water at the cooling tower exit is

$$\chi_0 = \frac{Q}{\pi R^2 V_0} \tag{A-11}$$

where R is the radius of the tower exit and V_0 is the exit velocity of the air from the tower. Combining Eqn.A-10 at the exit and A-11, then

$$\sigma_y^0 \sigma_z^0 = \frac{R^2 V_0}{2u} \tag{A-12}$$

where σ_y^0 and σ_z^0 are the initial values of σ_y and σ_z at the top of the cooling tower.

Using A-10 for distances downwind shorter than that at which σ_z^0 becomes comparable to the distance of the plume from the ground or the top of the "mixing layer," the dilution ratio along the plume centerline is given by

$$\frac{\chi_0}{\chi} = \frac{\sigma_y \sigma_z}{\sigma_y^0 \sigma_z^0} \tag{A-13}$$

When this ratio rises to R_d, the centerline concentration falls below saturation and the plume disappears.

As an example, consider once again a case for the cooling towers of the Tomsk-7 reactors: cooling capacity = 0.3 MWth/m^2; h = 60m, R= 30 m, V_o = u= 4m/s; and T_o 0.2 °C lower than the temperature at which it leaves the pack with 100% saturation. For an ambient air temperature of 20 °C and 80 percent humidity, the critical dilution factor at the end of the visible plume estimated from A-8, A-9, Figure A-1,and Eq. A -1 is about 4. The corresponding length of the plume can be estimated using Eq. A-13 and A-10 to be 50m, 200m and 500m for weather classes A,D and F respectively. Figure A-3 shows the actual shapes of the plumes as seen from above. For the same cooling tower performance and weather state as above, except for a change of the relative humidity to 50 percent, these lengths would be reduced to 20m, 80m and 200m respectively.

Using such calculations it can be concluded that, under almost all weather and operating conditions, a plume of condensed water vapor will be visible at least at the exits of operating natural-draft cooling towers. With low relative ambient humidity and high air temperature, such plumes are short and

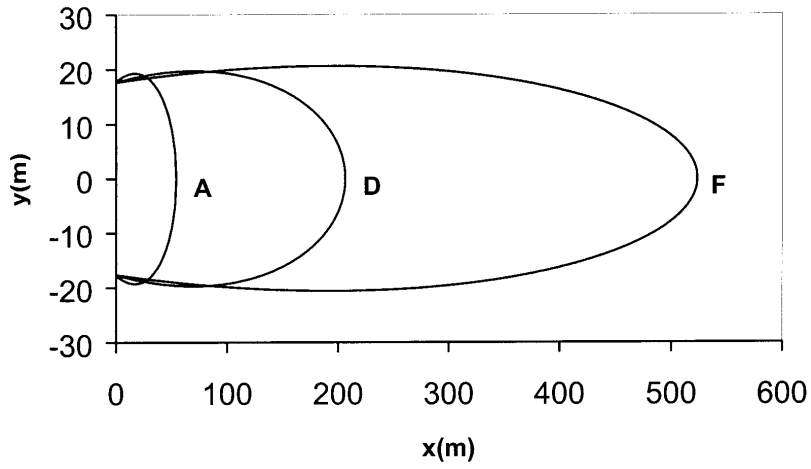

Figure A-3: Horizontal center-line cross-sections of the visible plume calculated for a Sev-ersk cooling tower under Pasquill A,D and F dispersal conditions. (x,y) are the downwind and crosswind distances from (0,0), the location of the tower top (which has a radius of 15 m). For ambient air temperature 20 ^{o}C and relative humidity 80%.

quickly dispersed. During periods of low wind speed and high humidity or low air temperature, the plumes may be very dense and can extend for several kilometers downwind before disappearing.

Appendix B. Detectability of objects smaller than the instantaneous field of view of a TIR pixel

A surface radiates a total energy flux of $S = \varepsilon\sigma T^4$ Watts/m^2 where ε is the emissivity of the surface, σ is the Stefan-Boltzmann constant [5.67×10^{-8} $Watts/(m^2 \cdot {}^\circ K^4)$], and T is the absolute temperature of the body. Most non-metallic surfaces have thermal emissivities between 0.85 and 1(ε = 1 for a black body).[48] The total power radiated from an area (A) of the surface is then:

$$P = \varepsilon\sigma T^4 A \qquad \text{(B-1)}$$

If the area of a hot object A intersected by the instantaneous field of view (IFOV) of the pixel (A_p) of a satellite TIR detector is smaller than A_p, the effective temperature increase seen by the detector will be an area-weighted average with the background temperature:

$$\varepsilon T^4 f + \varepsilon_b T_b^4 (1 - f) = \varepsilon_b T_{eff}^4 \qquad \text{(B-2)}$$

where ε_b and T_b are the background emissivity and temperature respectively and $f = A/A_p$ is the fraction of the pixel IFOV covered by the hot surface.

Solving B-2 for values of $T_r - T_b$ small in comparison with the absolute temperature T_b gives

$$\Delta T_{eff} \equiv T_{eff} - T_b \approx \{(\varepsilon/\varepsilon_b)(T - T_b) + (1/4)[(\varepsilon/\varepsilon_b) - 1] T_b\} f \qquad \text{(B-3)}$$

In order to be detectable, ΔT_{eff} must be greater than the threshold sensitivity of the TIR detector, ΔT_{th}. In the approximation $\varepsilon = \varepsilon_b = 1$ and using B-3 this condition becomes

$$A(T - T_b) \geq A_p \Delta T_{th} \qquad \text{(B-4)}$$

As an extreme example, consider the detectability of vapor plumes if they were visible only inside the tops ot the Tomsk-7 reactor cooling towers – as nearly appears to be the case for some of the Tomsk-7 cooling towers in Figure 3. We have estimated in Appendix A that, for an ambient air temperature of 20 °C and 50 percent humidity, the temperature difference between the input and output air of the cooling tower would about 14.5 °C. The area of a single

tower top is about 700 m^2. If the ground temperature is also 20 °C, $A(T\text{-}T_b) \approx 10^4\ m^2 \cdot °C$. At the Jiuquan reactor the individual tower tops have about half the area of those at Tomsk-7, i.e. $A(T - T_b) \approx 5,000\, m^2 \cdot °C$, For comparison, according to Table 4, $A_p T_{th}$ for the TIR detectors on Landsat-5, 7 and ASTER are: 7-14,000, 2-4,000, and 1,600 $m^2 \cdot °C$ respectively. It therefore appears that, even if a plume covers an area no bigger than the top of a Tomsk-7 or Jiuquan cooling tower, it should be detectable by the TIR detectors on Landsat-7 and ASTER. However, its detectability by the TIR detector on Landsat-5 would depend on the effective size of the plume and its temperature difference with the ground.

It will be seen from B-3, however, that ΔT_{eff} can also be above threshold, even if there is no temperature difference, if there is a significant difference between the thermal emissivities of the roof and background, . For the case $T_r = T_b$, if f = 1 and T_b = 300 °K, ΔT_{eff} = 1 °K if there is more than a 1.3 % difference in the emissivities. For a surface such as the roof of a GDP, a comparison of ΔT_{eff} for a still and a windy day will therefore be useful to determine how much of ΔT_{eff} is due to a real temperature difference and how much due to an emissivity difference. On a windy day, T_r -T_b would be reduced by a significant factor due to enhanced convective cooling [see the discussion of the two TIR images of the Portsmouth GDP (Figures 4c and d) in the main text].

Based on B-1, the difference in the power radiated from the roof and the background per unit area due to the elevated temperature of the roof is

$$\Delta P_r \approx 4\sigma\varepsilon_b T_b^3 \Delta T_{eff} \text{ Watts/m}^2 \qquad \text{(B-5)}$$

In the approximation ε_b= 1 , T_b = 300 °K, this gives ΔP_r= $6\Delta T_{eff}$ Watts/m^2.

Appendix C. Sizing Cooling Ponds[49]

For a given surface area, the most efficient cooling pond is deep enough to allow density currents to spread the warm water effluent easily over the surface of the pond. The water inlet should be located at the coolest point of the pond surface, and there should be minimal mixing of the hot water with the cooler deep water to ensure the warmest possible surface layer temperature for a maximal surface cooling rate.[50] The time required for water to pass through the pond depends on the pumping rate and the pond volume while the temperature drop from the plant discharge to the plant intake depends on the pumping rate and the pond surface area. Since the water surface temperature varies with distance from the discharge point, the heat transfer rate from the pond surface is not uniform.

The heat transfer rate from the pond surface is

$$P = \int K(T_s - T_e)\,dA \text{ Watts} \qquad \text{(C-1)}$$

where K is the surface heat exchange coefficient in Watts/m^2-°C, A= pond surface area in m^2, and T_s and T_e are respectively the local and equilibrium surface temperatures in °C.

The equilibrium temperature is the water surface temperature at which there is no net heat transfer from the water surface to the atmosphere and (by radiation) to space. The surface heat exchange coefficient depends on the wind speed, temperature and wet-bulb temperature (T_{wet}) of the air above the pond and has been parameterized as follows:[51]

$$K = 3.7 + 3.97(1 + 0.05V^2)(1.04 + 0.761T' + 0.0026T'^2) \quad W/m^2 \cdot °C \qquad \text{(C-2)}$$

where V is the wind velocity in m/sec and T'=(T_s+T_{wet})/2. The surface heat exchange coefficient generally ranges between 20-40 $Watts/(m^2 \cdot °C)$.[52]

In a steady-state, steady-flow condition, this heat dissipation rate is equal to the difference between the heat flow into the pond and the heat out of the pond. In terms of the plant intake temperature (T_i) and discharge temperature(T_d) (°C), it is

$$P = C_w \rho J_w \Delta T \quad \text{Watts} \qquad \text{(C-3)}$$

where ρ is the water density (1000 kg/m^3), C_w is the specific heat of water $4200\,j/(k\,g \cdot °C)$, J_w is the water flow rate in m^3/sec, and $\Delta T = T_d - T_i$. For $\Delta T = 15°C$, J_w = 16 (m^3/sec)/GWth.

Given a steady-state, steady-flow condition, one can equate (C-1) and(C-3)

$$C_W \rho J_W (T_d - T_i) = \int K(T_s - T_e)\,dA \qquad \text{(C-4)}$$

One can also apply this same equation to the water flow through and the heat loss rate from a strip of the surface of the pond with an average temperature T_s and a temperature difference dT_s between its upstream and downstream sides to get the differential equation

$$C_W \rho J_W dT_s = K(T_s - T_e)\,dA \qquad \text{(C-5)}$$

C-5 integrates to

$$\ln[(T_d - T_e)/(T_i - T_e)] = KA/(C_W \rho J_W) \qquad \text{(C-6)}$$

Combining C-6 and C-3 gives the pond area per MWth required to achieve a given cooling ratio

$r \equiv (T_d - T_e)/(T_i - T_e)$

$$A/P = (1nr)/[K(T_d - T_i)] \text{ km}^2/\text{MW} \qquad \text{(C-7)}$$

NOTES AND REFERENCES

1. Steven Fetter and Frank von Hippel, "A Step-by-Step Approach to a Global Fissile Materials Cutoff," *Arms Control Today* 25 (October 1995): No. 8, 3-8.

2. Mark Hibbs, "China Said to be Preparing for Decommissioning Defense Plants," *Nuclear Fuel*, May 17, 1999. See also David Albright, Frans Berkhout and William Walker, *Plutonium and Highly Enriched Uranium 1996-World Inventories, Capabilities and Policies* (Oxford University Press, 1997).

3. U.S. KH-12 satellites, first launched in November 1992, can reportedly achieve 10cm-resolution images at visible wavelengths. They also carry thermal infrared (TIR) imaging systems. If a thermal infrared system uses the same optical system, its resolution could be as good as 2 meters (www.fas.org/spp/military/program/imint/kh-12).

4. M. Krepon, et. al., *Commercial Observation Satellites and International Security*, (New York: St. Martin's Press, Inc., 1990); M. Slack and H. Chestnutt, *Open Skies -- Technical, Organizational Operational, Legal and Political Aspects*, (Canada: York University, 1990); M. Krepon, et. al., *Open Skies, Arms Control, and Cooperative Security*, (New York: St. Martin's Press, Inc., 1992).

5. See e.g. www.fas.org/nuke/guide/russia/facility/nuke/index.

6. The KH-4B cameras took images on photographic film. For such system, the most common definition of resolution is based on the number of equidistant dark bars in a standard resolution target which can be resolved per millimeter of film. Approximately one line-pair is necessary to detect an object. The spatial resolution definition used in this paper is that used for electro-optical sensors, the size of the smallest ground area sampled by the system detector element, a "pixel." This is referred to as the "instantaneous field of view" (IFOV). Approximately two pixels are required to present the same amount of ground information as one line pair at "normal" film contrast. Therefore, the 1m (3ft) resolution images (one pixel) of the commercial satellites are comparable to those 1.8m (6ft) resolution images of KH-4B. It should be noted, however, that, using modern digital image processing techniques, the 1-m resolution images of those new commercial satellites can be made clearer than the unprocessed images from the KH-4B satellites.

7. Kam W. Li and A. Priddy, *Power Plant System Design* (John Wiley & Sons,1985).

8. The production of one kg of weapon-grade uranium with 0.25% U^{235} left in the depleted uranium "tails" requires about 208 kilogram-Separative Work Units (kg-SWU). A typical GDP generally requires between 2.3 and 3 megawatt hours for every kg-SWU produced, S. Villani, "Uranium Enrichment" in *Topics in Applied Physics, Vol. 35*, (Springer-Verlag, New York, 1979), p.167-170. The separative work D, in kg-separative-work units (SWUs) is given by $D = WV(e_w) + PV(e_p) - F(e_f)$ where P is the mass of product in kg, W of waste depleted uranium, and F of feed – all in kg. $V(e) = (2e - 1)\ln[e/(1-e)]$ and e_p, e_w, and e_f are the fractional enrichments of the product, waste and feed streams. $F = P(e_p-e_w)/(e_f-e_w)$ and $W = P(e_p- e_f)/(e_f- e_w)$.

9. J. Weisman, R. Eckart, *Modern Power Plant Engineering* (Prentice-Hall, Inc.,1985).

10. Heating a kg of dry air at 20 °C by 10 °C absorbs 10 kj. Adding water to keep it saturated requires the evaporation of 12 grams of water, absorbing an additional 28 kj.

11. Israel's Dimona reactor and Pakistan's Khushab reactor use mechanical-draft cooling towers.

12. See http://www.fas.org/nuke/guide/russia/facility/nuke/index.html.

13. EI-2 operated from Sept 1958 to Dec 1990 and produced an estimated 10 tons of weapon-grade plutonium (WgPu). ADE-3 operated from July 1961 to Aug 1992 and produced an estimated 14 tons WgPu. Nils Bohmer and Thomas Nilsen, Seversk (Tomsk-7) (*Bellona Working Paper*, No.4,1995); *Plutonium and Highly Enriched Uranium* 1996.

14. Private communication, Oleg Bukharin, Center for Energy and Environmental Studies, Princeton University,1999.

15. From the recent declassified collection of KH-1 to KH-6 photos for the period 1960 to 1972. This photo was taken by the KH-4B satellite. A directory to these photos was shown on the U.S. Geological Service web site at http://edcwww.cr.usgs.gov/glis/hyper/guide/disp.

16. It should be noted that, with a snow background, it would be difficult to distinguish the vapor plumes (beyond the tops of towers) from the snow because they have very similar spectral response in the VNIR region (wavelengths from 0.4 to 1.3 μm). However, they can be easily differentiated in the middle-infrared portion of the spectrum (1.3-3 μm), particularly in the 1.55 to 1.75 and 2.10 to 2.35 μm wavelength bands. In these bands vapor plumes have a very high reflectance and appear white while snow has a very low reflectance and therefore appears dark in the imagery. Thus low-resolution multispectral scanners (such as those of Landsat TM) could be used to distinguish vapor plumes from snow in winter. See also, Roger M. Hoffer, "Biological and Physical Considerations in Applying Computer-aided Analysis Techniques to Remote Sensor Data," in Swain, P.H. and S. M. Davis (ed), *Remote Sensing: The Quantitative Approach* (New York :McGraw Hill, 1978), 227-289.

17. The burnup required to produce weapon-grade plutonium in natural-uranium fueled production reactors is about 1000 MWt-days/ton. Power reactors are designed to fission most of the U-235 in their fuel. This corresponds to burnups of about 7000 MWt-days/ton for natural-uranium-fueled power reactors and 30,000-60,000 MWt-days/ton for reactors fueled with 3-6 percent enriched uranium.

18. The equilibrium time for a uranium enrichment cascade is the time required to reach the first production of uranium at the design product assay, starting with the cascade initially filled with inventory at the feed assay.

19. http://www.fas.org/nuke/guide/pakistan/facility/khushab.htm.

20. A test was carried out by the Carnegie Endowment's Nonproliferation Project in which Landsat-5 TIR images of the area around the 60 MWt research reactor operated at Brookhaven National Lab were obtained for two days -- one when the reactor was operating, and one when it was not. The reactor uses closed-cooling towers (presumably wet-type cooling towers) to dissipate heat. The images did not show convincing evidence of a thermal signature when the reactor was operating. See Leonard S. Spector, "Monitoring Nuclear Proliferation," in *Commercial Observation Satellites and International Security*, ed. Michael Krepon, et al., Carnegie Endowment for International Peace, 1990. This result is consistent with our calculations in appendix B. However, the probability of detection should be high with a high-resolution TIR satellite such as ASTER.

21. L.C.Wilbur, *Handbook of Energy System Engineering: Production and Utilization* (John Wiley & Sons, 1985).

22. "*United States Army Multispectral Imagery Product Guide,*" Second Edition, ATC-IA-2681-030-94, May 1994.

23. Bhupendra Jasani and Alan Blackburn, "Piercing into Secret Nuclear Establishment Using Imagery from Civil Satellites," in *Proceedings of the 21st Annual Conference of the Remote Sensing Society,* 11-14 Sept, 1995, Paul Curran and Colette Robertson, eds.

24. Frank von Hippel, D.A. Albright and B.G. Levi, "Stopping the Production of Fissile Materials for Weapons," *Scientific American*, September 1985.

25. The nearby Krasnoyarsk hydropower plant is rated at 6 GWe. If the height of the dam is 100 meters, this corresponds to a flow at 90 % conversion efficiency of 7,000 m^3/ sec.

26. S. Villani, op cit.

27. For example, in France's Tricastin GDP, the air temperature in sections of the building containing the cascades must be kept at 80°C (176°F) (see M. Molbert, "The Eurodif Program," in *Recent Developments in Uranium Enrichment*, J.R. Merriman,et al, eds. (New York: American Institute of Chemical Engineers, 1982) Vol.98, 221.

28. Subsequent to the completion of this paper, a more detailed analysis of these TIR images was carried out by Adam Bernstein. A. Bernstein, *Monitoring Large Enrichment Plants Using Thermal Imagery from Commercial Satellites: A Case Study* (Sandra National laboratories, report SAND 2000-8671, 2000), 15.

29. Building X-333, which contains 640 stages, is 25 m high, and has an area of 0.1 km^2 (440 m x 300 m). Typical operating temperature and high-side pressures for the process gas in this building are in the range 127-140 °C and 0.35-1 atmospheres. Building X-330, housing 1100 stages of intermediate size, is 20 m high and has an area of 0.13 km^2 (660 m x 200 m). Finally, building X-326, housing 2280 small-size stages including the high-enrichment end of the cascade, is 19 m high, and has an area of 0.12 km^2 (680 m x 170 m). Brookhaven National Laboratory, *Transparency Measures for DOE SNM Production Facilities*, SSN 93-7 (December 1993).

30. For an emissivity of unity, the blackbody radiation heat loss at 20 °C is about 6 (T_r – T_s) Watts/ m^2 where T_r is the roof temperature and T_s is the radiation temperature of the sky. The convective heat loss has been estimated at (5.7 + 3.8V)(T_r –T_a) Watts/m^2 where V is the wind velocity in m/sec and T_a is the air temperature [John A. Duffie and

William A. Beckman, *Solar Energy Thermal Processes* (John Wiley & Sons, 1974), p. 83]. Approximating $T_s = T_a$, the summed surface heat loss coefficient, $C_S = 11.7 + 3.8V$ Watts/(m^2-°K) would increase roughly threefold from a still air situation to one with a wind velocity of 6 m/sec (13.5 mph). If the heat flow through the roof is controlled dominantly by the conductivity of the roof material [about 0.5 Watts/(m^2-°K) for 10 cm of insulation], this wind effect would lower the temperature difference $T_r - T_a$ by a factor of three.

31. *Plutonium and Highly Enriched Uranium 1996: World Inventories, Capabilities and Policies*, 127.

32. The Lanzhou GDP reportedly ended HEU production in 1987 (see Table 2). But it may have been producing LEU in 1989.

33. International Nuclear Fuel Cycle Evaluation, INFCE/PC/2/2, *Enrichment Availability*, (IAEA, Vienna,1980), 133.

34. *Plutonium and Highly Enriched Uranium 1996: World Inventories, Capabilities and Policies*, 275.

35. B. Jasani, et al, *Enhancing IAEA Safeguards Using Commercial Satellite Imagery – A Pilot Study*, November 1996, (University of London, Department of War Studies, UK and the Federal Republic of Germany Safeguards R&D Programmes, SRDP-R-240, JOPAG/12.95-PRG-265, Task A.16/JNT D882, 1996).

36. U.S. Congressional Office of Technology Assessment, *Building Energy Efficiency* (1992), 24.

37. B. Jasani, et al, *Enhancing IAEA Safeguards Using Commercial Satellite Imagery – A Pilot Study*.

38. Hui Zhang, "A View on the Application of Overhead Imagery to strengthen the IAEA Safeguards Regime," in *Arms Control and The Rule of Law: A Framework for Peace and Security in Outer Space*, J. Beier and S. Mataija, eds (Toronto: York University, 1998).

39. N.P. Cheremisinoff, et al., *Cooling Towers: Selection, Design and Practice* (Ann Arbor Science Pulishers, Inc.,1981); W. Stanford and G. Hill, *Cooling Towers: Principles and Practice* (England Carter Industrial Products Limited, 1972); R. Woodson, "Cooling Towers," *Scientific American*, May 1971; W. Maze, "Practical Tips on Cooling Tower Sizing," *Hydrocarbon Process*, (1967), No. 2.

40. F.R. Barber, et al., "The persistence of plumes from natural draught cooling towers," *Atmo. Envir. 8* (1974), p. 407. For unsaturated air, the temperature of the rising air would decline as Mg/(9R/2) = 0.0077 °C/m where M is the molar mass of air (0.029 kg), g the gravitational constant (9.8 m/sec^2) and R the molar gas constant [8.3 $j/(mole \cdot °K)$]. However, the heating effect of the condensing water vapor would offset this effect. At 25 °C, for example, cooling by 1 °C will reduce the amount of water carried by a kg of saturated air by 1.2 grams, which would release 2.9 kj of heat -- enough to raise the temperature by 2.9 °C. The net result would therefore be to reduce the cooling for saturated air at this temperature to about 0.0028 °C/m.

41. G. Csanady, "Bent-Over vapor plumes," *J. Appl. Meteor.* 10 (1971), 36.

42. *Cooling tower plume modeling and drift measurement*, (New York: The American Society of Mechanical Engineers, 1975).

43. Typically about twice the top diameter.

44. L. Wilbur, et al., *Handbook of Energy Systems Engineering: Production and Utilization* (John Wiley & Sons, 1985).

45. Assuming that each tower has a cooling capacity of 200 MWt on the basis of the number of cooling towers per reactor and the reported rated thermal powers of the reactors.

46. See e.g. D. Bruce Turner, *Workbook of Atmospheric Dispersion Estimates: An Introduction to Dispersion Modeling*, (CRC press, 1994). The second term in the curly brackets in A-10 accounts for the reflection of plume off the ground.

47. A. Green, et al., "Analytic extensions of the Gaussian plume model," *JAPCA*, Vol.30, (1980) No.7. For x less than about a kilometer, we may approximate $\sigma_y \approx k_y x$, $\sigma_z \approx k_z x$ with k_y = 0.25, 0.08 and 0.04 and k_z = 0.1, 0.05 and 0.02 for A, D and F-type stability conditions respectively. For a source of significant size, such as the present case, the values of x must be replaced by $x + x_y$ and $x + x_z$ with x_y and x_z chosen so that σ_y and σ_z have the correct initial values at x = 0. Assuming that $\sigma_y(0) = R/\sqrt{2}$, from (A-13), $\sigma_z(0) = (V_o/u)\ (R/\sqrt{2})$.

48. *1993 ASHRAE Handbook: Fundamentals* (American Society of Heating, Refrigerating and Air-Conditioning Engineers, 1993), 3, 8.

49. K.W. Li and A. Priddy, *Power Plant System Design* (John Wiley & Sons, 1983); G. Jirk, et al.,"Steady State Estimation of Cooling Pond Performance," *J. Hydraulics Division, ASCE* 106 (HY6) (June 1980).

50. G. H. Jirka, et al., "Cooling Impoundments: Classification and Analysis," *J. Energy Division, American Society of Civil Engineers*, Vol.105 (Aug.1979), No. EY2.

51. D.K. Brady, et al., "*Surface Heat Exchange in Power Plant Cooling Lakes*," research report, John Hopkins University Press,1969; K.W. Li and A. Priddy, op cit. The wet-bulb temperature T_{wet} is determined implicitly by the temperature T_{air} and fractional humidity f_{air} of the air as $T_{wet} = T_{air} + 2400\{[1 - f_{air}]\ F_{ws}(T_{air}) - F_{ws}(T_{wet})\}$, where $F_{ws}(T)$, the fractional weight of water in saturated air, is given by equation (A-9). 2400 is the ratio of the vaporization energy of water in to the specific heat of dry air in $j/(g\,m \cdot {}^\circ C)$.

52. D.K. Brady, et al, *op cit*.